SYNTHESIS AND CHARACTERIZATION OF SENSOR MICROPARTICLES TEMPLATED FROM CHOLESTERIC LIQUID CRYSTALS

A THESIS SUBMITTED TO
THE GRADUATE SCHOOL OF NATURAL AND APPLIED SCIENCES
OF
MIDDLE EAST TECHNICAL UNIVERSITY

BY

DENİZ IŞINSU AVŞAR

IN PARTIAL FULFILLMENT OF THE REQUIREMENTS
FOR
THE DEGREE OF MASTER OF SCIENCE
IN
CHEMICAL ENGINEERING

AUGUST 2020

Approval of the thesis:

SYNTHESIS AND CHARACTERIZATION OF SENSOR MICROPARTICLES TEMPLATED FROM CHOLESTERIC LIQUID CRYSTALS

submitted by **DENİZ IŞINSU AVŞAR** in partial fulfillment of the requirements for the degree of **Master of Science** i**n Chemical Engineering, Middle East Technical University** by,

Prof. Dr. Halil Kalıpçılar
Dean, Graduate School of **Natural and Applied Sciences** _____

Prof. Dr. Pınar Çalık
Head of the Department, **Chemical Engineering** _____

Assist. Prof. Dr. Emre Büküşoğlu
Supervisor, **Chemical Engineering, METU** _____

Examining Committee Members:

Prof. Dr. Nihal Aydoğan
Chemical Engineering, Hacettepe University _____

Assist. Prof. Dr. Emre Büküşoğlu
Chemical Engineering, METU _____

Assoc. Prof. Dr. Mustafa Serdar Önses
Materials Science and Engineering, Erciyes University _____

Assoc. Prof. Dr. Pınar Zeynep Çulfaz-Emecen
Chemical Engineering, METU _____

Assist. Prof. Dr. Simge Çınar
Metallurgical and Materials Eng., METU _____

Date: 21.08.2020

I hereby declare that all information in this document has been obtained and presented in accordance with academic rules and ethical conduct. I also declare that, as required by these rules and conduct, I have fully cited and referenced all material and results that are not original to this work.

Name, Last name : Deniz Işınsu Avşar

Signature :

ABSTRACT

SYNTHESIS AND CHARACTERIZATION OF SENSOR MICROPARTICLES TEMPLATED FROM CHOLESTERIC LIQUID CRYSTALS

Avşar, Deniz Işınsu
Master of Science, Chemical Engineering
Supervisor : Assist. Prof. Dr. Emre Büküşoğlu

August 2020, 64 pages

Structural coloring in nature, especially the crystalline ordering and responsive characteristics of those found in chameleon skins has inspired us to fabricate artificial photonic materials for sensor applications. In the first part of this study, we employed cholesteric liquid crystals (CLCs) for templated synthesis of polymeric particles with periodic structures that allow visible light to undergo Bragg reflection and performed characterization studies to understand the optical appearance and the internal structure of the polymeric particles to be used as sensors. In the second part, we tested their response against volatile organic compounds (VOCs) and quantified the optical response by including colorimetric imaging. We demonstrated that the particles were responsive against toluene with detection limits, surprisingly in the order of 100 ppm. Then, we investigated the response characteristics and determined the critical role of the liquid crystal elasticity in the response of particles upon VOCs exposure. We found that such a high sensitivity was achieved due to the critical steps we followed during the CLC-templated synthesis of particles that resulted in the storage of an elastic energy in the anisotropic polymer network. In addition to the

sensor tests, we presented our efforts to design particle-assisted sensor chips that allow easy integration into wearable optical devices for easy and reliable online tracking of VOC concentrations. The results proved that sensors developed from the CLC-templated particles can be used multiple times without a significant loss of sensitivity and offered rapid, sensitive and battery-free detection.

Keywords: Cholesteric Liquid Crystals, Structural Coloring, Elastic Energy, Optical Gas Sensor, VOCs

ÖZ

KOLESTERİK SIVI KRİSTAL ŞABLONLU SENSÖR MİKRO PARÇACIKLARIN SENTEZİ VE KARAKTERİZASYONU

Avşar, Deniz Işınsu
Yüksek Lisans, Kimya Mühendisliği
Tez Yöneticisi: Assist. Prof. Dr. Deniz Işınsu Avşar

Ağustos 2020, 64 sayfa

Doğadaki yapısal renklenme, özellikle bukalemun derilerinde bulunanların kristal düzeni ve duyarlı özellikleri sensör uygulamaları için yapay fotonik malzemeler üretmemize ilham verdi. Bu çalışmanın ilk bölümünde, görünür ışığın Bragg yansımasına izin veren periyodik yapılara sahip polimerik mikro parçacıkların şablon sentezi için kolesterik sıvı kristalleri kullandık ve sensör olarak kullanılacak bu mikro parçacıkların optik görünümü ve iç yapısını anlamak için karakterizasyon çalışmaları gerçekleştirdik. İkinci bölümde ise polimerik mikro parçacıkların uçucu organik bileşiklere (UOB) karşı tepkilerini test ettik ve optik yanıtı kolorimetrik görüntüleme ile nicelleştirdik. Şaşırtıcı bir şekilde parçacıkların 100 ppm mertebesinde tolüen gazına karşı duyarlı olduklarını gösterdik. Daha sonra tepki karakteristiğini araştırdık ve parçacıkların UOB maruziyeti ile tepkisinde sıvı kristal elastikiyetinin kritik rolü olduğunu belirledik. Böyle yüksek bir hassasiyetin, kolesterik sıvı kristal şablonlu parçacık sentezi sırasında izlediğimiz, elastik enerjinin anizotropik polimer ağında depolanmasıyla sonuçlanan kritik adımlar sonucu elde edildiğini bulduk. Son olarak bu çalışmada, sensör testlerine ek olarak uçucu organik bileşiklerin kolay ve güvenilir çevrimiçi takibi için giyilebilir optik cihazlara kolay uyum sağlayan parçacık destekli sensör çipleri tasarlama

çalışmalarımızı sunduk. Sonuçlar, kolesterik sıvı kristal şablonlu parçacıklardan geliştirilen UOB sensörlerinin, önemli bir hassasiyet kaybı olmadan birden çok kez kullanılabileceğini ve hızlı, hassas ve pilsiz algılama sunduğunu kanıtlamıştır.

Anahtar Kelimeler: Kolesterik Sıvı Kristal, Yapısal Renklilik, Elastik Enerji, Optik Gaz Sensörleri, UOB

To my mom and dad

ACKNOWLEDGEMENTS

I would first like to say a special thank you to my supervisor, Asst. Prof. Dr. Emre Büküşoğlu, whose expertise was invaluable in the formulating of the research topic and methodology in particular. His support, guidance, encouragements and overall insights in this field have made this an inspiring experience for me. I must also express my gratitude to our cluster; Assoc. Prof. Dr. P. Zeynep Çulfaz Emecen, Assoc. Prof. Dr. Erhan Bat, and Asst. Prof. Dr. Simge Çınar.

From the bottom of my heart, I would like to say big thank you for all the Soft and Functional Materials Research Group members; Aslı Karausta, Burak Akdeniz, Ceren Kocaman, Elif Kurt, Özge Batır, Selin Şengül and Umut Dinç for their friendship, interdependency, support, and help throughout my project. They are more than lab mates to me. I feel lucky for being met with you all and having spent all that time together. I also would like to thank my dear friends Tutku Kartal, Toprak Çağlar, Deniz Sönmez, Cansu Civelek and Melis Kırarslan for their endless support, friendship, encouragements and as well as providing happy distraction to rest my mind outside of my research.

Last but not the least, my biggest thanks to my family for their wise counsel, all the unconditional love and support in this very intense academic journey. They kept me going on and this work would not have been possible without their input. Sorry for being even grumpier than usual while I wrote this thesis during lockdown times! And, I am grateful to my dearest Ahmet Güçbilmez for his endless love, patience, support and sympathetic ear.

For financial supports, I would like to thank the Scientific and Technological Research Council of Turkey (TÜBİTAK) under the award number 217M268.

TABLE OF CONTENTS

LIST OF FIGURES

FIGURES

LIST OF ABBREVIATIONS

ABBREVIATIONS	
LC	Liquid Crystal
CLC	Cholesteric Liquid Crystal
LCE	Liquid Crystal Elastomers
VOC	Volatile Organic Compound
CV	Coefficient of Variance

CHAPTER 1

INTRODUCTION

We experience the world by interpreting colors. Colors have great importance in the survival and daily activities of living organisms such as social interactions, predation, signal communication, sexual selection, and camouflage.[1,2] Color creation mostly arises from the interaction of visible light (absorption, reflection, and scattering) with pigments or periodic structures. Pigmentary colors rely on the selective light absorption by the electrons of pigments. When the incident light strikes a pigment molecule, electrons are excited to a higher state as a result of energy exchange between the light and electrons. Thus, the selective wavelengths of light are absorbed while others are allowed to be reflected, and coloration is achieved. The colors owing to the presence of periodic structures called structural colors. In this case, coloration relies on selective light reflection through purely physical phenomena of light such as diffraction, interference, and scattering. In comparison with pigmentary colors, the structural colors are more efficient since the coloration mechanism does not include energy loss in the use of light. The structural colors do not fade over time like pigments as long as the periodic structures exist. The brightest and distinctive colors in nature are structural colors.[1–5]

Over half billion years of evolution, fascinating microstructures were revealed in many species such as peafowls, *Morpho* butterflies, hummingbirds, and marble berries which exhibit structural colors originating from periodic structures that possess length scales in the order of the visible light wavelengths.[2,4,6,7] Figure 1.1 shows a fascinating blue color of a typical *Morpho* butterfly and the scanning electron microscope (SEM) images of its inherent periodic structure. The wing scales of the butterfly comprise hundreds of periodically stacked ridges (Figure 1.1C),

which are the multilayer cuticle (lamella-air) structure with the shape of a ‘’Christmas tree’’ from the cross-section (Figure 1.1D). The shiny blue color of *Morpho* butterfly is simply a result of coherent scattering in blue wavelengths while canceling out or transmitting the other wavelengths through the wing.[4,8,9]

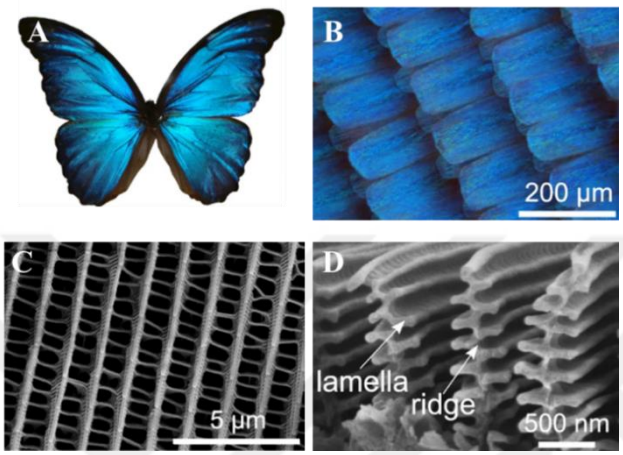

Figure 1.1 (A) *Morpho didius* butterfly showing distinctive blue coloration and (B) an enlarged view of a wing scales. A scanning electron microscope (SEM) image of (C) ridges on a single wing scale (top view) and (D) a cross-section of the ridges contains alternating layers of air and lamellas.[8]

These structures in living creatures are not only a significant feature resulting in distinctive appearance but also enable dynamic color changes.[2,4,10] Numerous examples of natural creatures with dynamic structural coloring exist and the color changing mechanisms are generally based on the modification of the periodicity of the nanostructures embedded in their body. For instance, the neon tetra fish reflects a structural color of cyan arises from periodically stacked platelets of guanine nanocrystals in their iridophore cells. Under stressful conditions, the reflected blue color changes to yellowish color. Researchers have suggested that the inflow of water through the iridophore cells leads to increasing the spacing between the platelets as illustrated in Figure 1.2A. This swelling results in selective reflection of a higher wavelength of the light.[2,11,12] Chameleons also demonstrate considerable ability to perform rapid color changes. A recent study have shown that the excitement during social interactions of chameleons causes active tuning of the distance between

guanine nanocrystals stacked in lattices and present as micrometer sized, colored domains embedded in their skin that result in a shift in the reflected color (Figure 1.2B).[13]

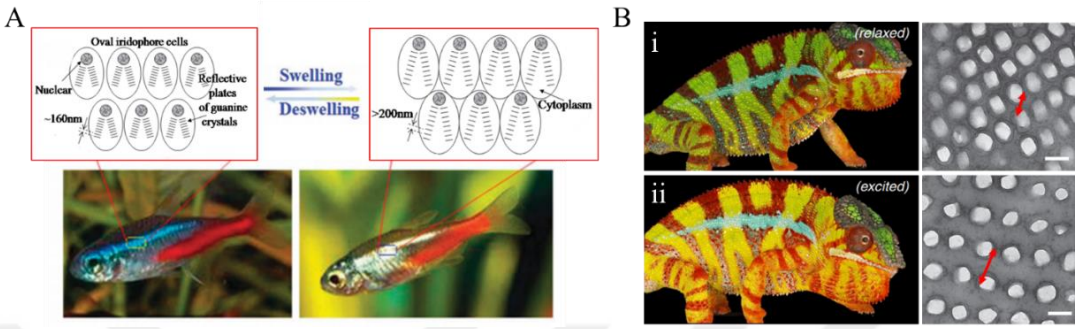

Figure 1.2 Natural creatures with dynamic color change: (A) The *neon tetra fish* normally displays a structural color of cyan, after the swelling of the oval iridophores, its stripe changes to yellow.[2,11] (B) Left images show the reversible colour change in a male chameleon from the (i) green to (ii) yellow/orange. Right images are transmission electron microscopy (TEM) images of the lattice of guanine nanocrystals in iridophores from the same individual in a (i) relaxed and (ii) excited state. Red arrows indicate the distance between guanine nanocrystals (Scale bars: 200 nm).[13]

Theoretically, Bragg's Law explained this natural ability by providing a direct relation between the reflected light of selective wavelength and periodicity of micro-nanostructures. The law considers a crystalline lattice in a vacuum that is composed of a regular arrangement of atoms with the distance of d (Figure 1.3).[10] When the light travels through the crystalline molecule, the incident beam is scattered by regularly spaced atoms and these scattered waves interfere constructively if they are in phase. According to Bragg's Law, as expressed in Equation 1, the condition for constructive interference is that the second reflected wave must travel an integer number of wavelengths.[3,4,10]

$$2d\cos\theta = m\lambda \qquad \text{Equation 1}$$

Where θ is the incident angle of the light, d is the spacing between atoms, λ is the wavelength giving the maximum reflectivity and m is an integer and the value m gives the 'order' of the diffraction.

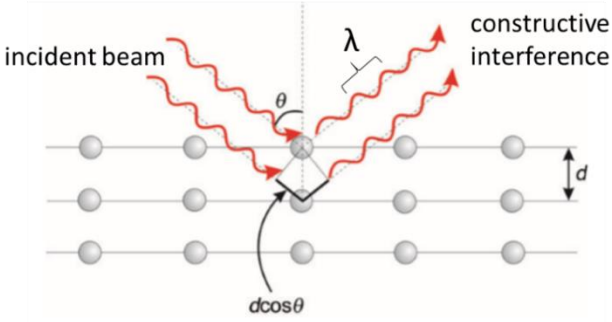

Figure 1.3 Simplified scheme of light reflection from ordered spheres by the explanation of Bragg's reflection.[10]

We were inspired by the energy-free color change mechanism of periodic nanostructures and aimed to apply this phenomenon to sensing technology that does not require any external energy. In this study, we sought to imitate periodic structures found in nature that appear with distinct coloring and exhibit dynamic response. We introduced liquid crystals (LCs) for the purpose of using the inherent periodicity of cholesteric liquid crystals (CLCs) to template low-cost, responsive polymeric particles to be used as volatile organic compound (VOC) sensors. LCs are a state of matter that exhibits fluidity of the isotropic liquid and also some anisotropic properties of crystalline solid such as refractive indices and long-range orientational ordering. LCs are classified as thermotropic if the liquid crystalline behavior occurs within a certain temperature range (Figure 1.4A).[14,15] The nematic phase is the simplest mesophase within the LC state, all of the rod-like mesogens exhibit an average direction which described by a unit vector termed the director, n. CLCs can readily be obtained by adding a chiral dopant in the nematic phase as shown in Figure 1.4B and characterized by a helical twist with axis orthogonal to the individual director of the constituent mesogens. The length of a 2π turn is called as pitch size (P) that is a function of the concentration, [c], of the chiral dopant through the following Equation:

$$P = \frac{1}{[c] \times HTP} \qquad \text{Equation 2}$$

where HTP is the helical twisting power of the chiral dopant, which quantifies the ability of a chiral dopant to twist the nematic.[16,17]

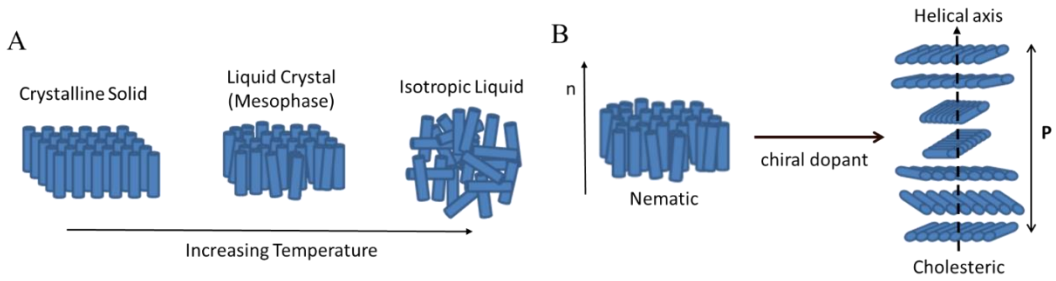

Figure 1.4 Schematic illustration of (A) the temperature-dependent phase transition of thermotropic LCs and (B) molecular arrangements of the nematic LC phase, and cholesteric LC phase obtained when a chiral dopant added to a nematic LC (n refers to nematic order and P refers to pitch size of helical structure) where the individual nematic layers stack together with a twist leading to helicoidal order with a pitch P, which refers to the distance over a full 360˚ twist.

The periodic structure of cholesteric phase allows the Bragg reflection of the selected wavelength of visible light if the pitch length is comparable to the visible light wavelengths (Figure 1.5A).[15,16] The selective reflection of light is governed by following equation:

$$\lambda = n \times P \times \cos\theta \qquad \text{Equation 3}$$

where λ is the wavelength of Bragg reflection, n is the average refractive index, the half-pitch P/2 replaces the thickness d in Equation 1 and θ is the angle of incident light.[16]

When helical pitch influenced by various external stimuli such as pH, temperature,[18] strain,[19] and chemicals, exhibit a change of reflected color (Figure 1.5B), which makes CLCs a perfect candidate for the usage in optical sensors.[17] However, the fluidic properties of CLCs hinder their practical use as sensors. Recent studies have shown that the ordering of the mesogenic constituents could be used to template polymeric materials with controlled nanostructure.[19–23]

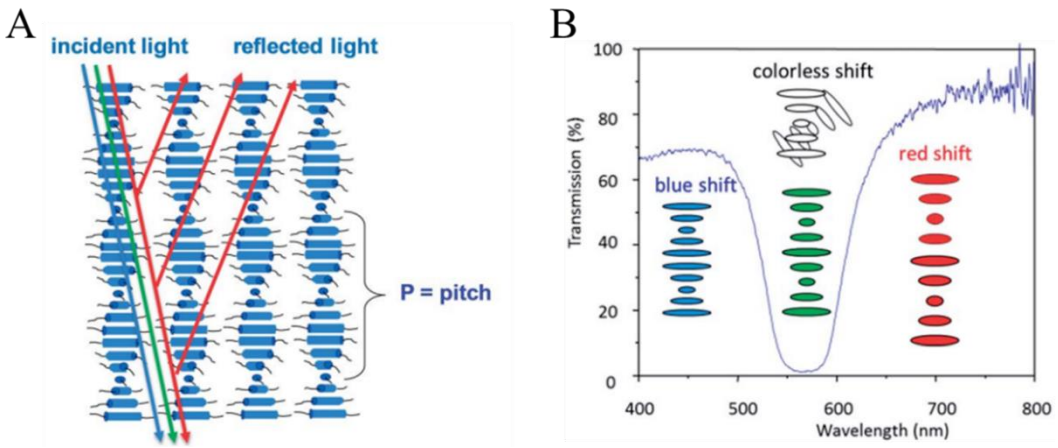

Figure 1.5 (A) The selective reflection of light by cholesteric liquid crystal (CLC). (B) Possible changes of the reflection band of a CLC structure upon external stimuli.[17]

Herein, we underline the two key concepts of LCs to better understanding the design parameters of this study. Figure 1.6A shows the surface anchoring which results from the intermolecular interactions between the mesogens and the interface. The ground state for the orientation of LC is the easy axis and the presence of external fields causes a deviation to the surface director, which leads to an increase in the interfacial free energy (F_s).[14,24] This idea allows to manipulation of the LC alignment such as planar and homeotropic by the chemical functionality of interface. Second idea is the elastic media of LCs which is related to the long-range orientational ordering. The expression in Figure 1.6B describes the energy storage in three strain states, which are splay, twist and bend, as a consequence of distortion to meet the confinement set by the surfaces.[14,24,25] In this study, we use CLCs to template the polymerization of particles, not only to obtain the structural coloring but also exploit their elastic media.

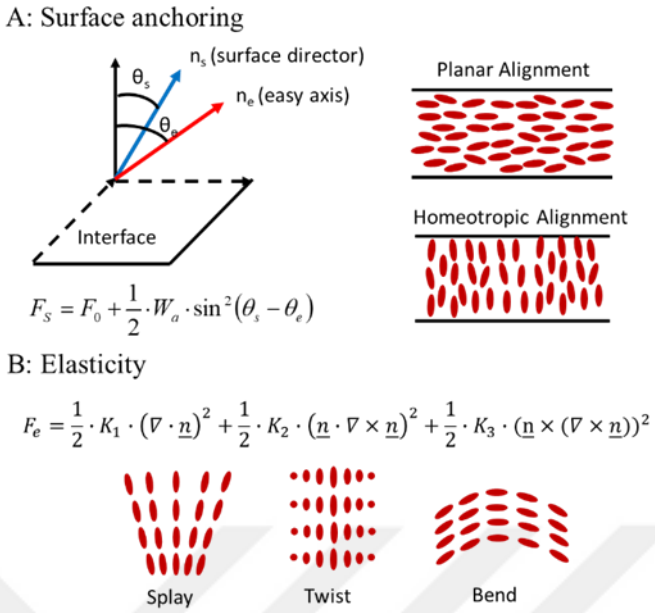

Figure 1.6 Schematic illustration of (A) the director and easy axis of a liquid crystal (LC) anchored at a surface and expression for the interfacial free energy (F_s) where F_0 is the free energy of the interface corresponding to the easy axis, Wa is the anchoring energy (typically 10^{-3}–10^{-2} mJ/m^2); (B) The three basic modes of deformation of a LC (splay, twist, and bend) and an expression of the free energy density (F_e) where K_1, K_2, and K_3 are splay, twist, and bend elastic constants, respectively (each typically in the order of 10^{-11} N).[14]

We are motivated towards sensing vapors of volatile organic compounds (VOCs). The reason behind building a VOC sensor is their presence in the environment due to their wide use especially in the industry and in daily life as they are released from burning fuels, paints, glues, industrial and household cleaners, etc. Despite these abundances, they constitute serious harm to human health such as causing infertility and neurological damages. Therefore, the early, reliable and fast detection of VOCs and continuous monitoring of their concentrations is essential. Also, the limit of detection is crucial since their threshold limits are set by the Occupational Safety and Health Administration. For example, permissible exposure limit of toluene is 200 ppm for an 8-hour time-weighted average and 500 ppm for a single period of up to 10 minutes.[26] Thus, an ideal sensor designed for such VOC should work between these concentration limits with a response time below minute scales.

CHAPTER 2

LITERATURE REVIEW

The most widely used commercial methods for the detection of VOCs comprise an efficient adsorbent combining with standard analytical chromatography techniques with either a flame ionization or with mass spectrometry, or photoionization detectors.[27,28] Although these methods provide precise and selective detection with the low limit of quantification (down to ppb or ppt levels), they are expensive and require bulky instruments and rendering the process of VOC detection time-consuming due to the transportation of analyte, adsorption/desorption rate and data transmission as a sensor output. Therefore, these systems are impractical for continuous in-situ monitoring of VOCs.[27–31] Advances in microfabrication allow micro-sized GC devices and many studies have been presented to date,[32–34]however, the high price of these devices limits their usage.[35] Recent studies have offered various types of methods that employ electrochemical, physical, and optical properties for VOC sensing. [30,31,35]Herein we describe the working principles of main sensor technologies such as electrochemical cells, photoionization detectors (PID), and resistive-based sensors.

Electrochemical sensors are classified as potentiometric and amperometric, according to either the sensor measurement is the potential difference or the electric current of an electrochemical reaction. The amperometric sensors contain a porous membrane that allows to analyte diffusion through the electrolyte as shown in Figure 2.1. The electric current is generated as a result of the redox reaction at the working electrode. This measured electric current becomes the sensor signal and is directly proportional to analyte concentrations.[31,35,36] Typically, this type of sensors have fast response time (~120s), low limit of detection down to ppb levels, and accurate

results. The selectivity and sensitivity can be optimized for a target VOC by changing the composition of electrodes. In general, these devices are disadvantageous in selectivity and durability.[35] Even low humidity leads to deviation of sensor signal and membranes may be degraded with time.[37]

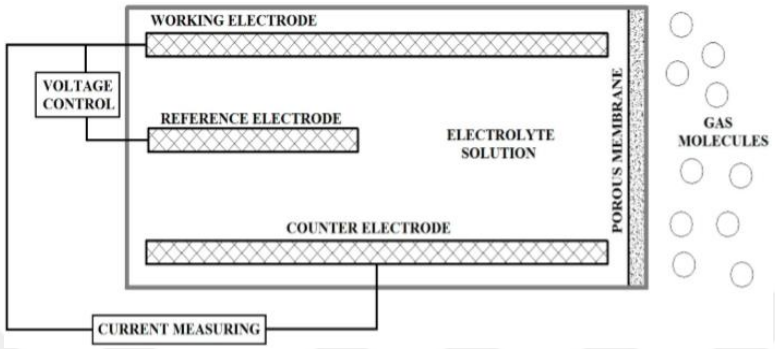

Figure 2.1 Schematic illustration of electrochemical (amperometric) sensor with the measurement (working) electrode, counter electrode and reference electrode.[31]

Photoionization detectors (PIDs) are the physical type of sensors since working mechanisms based on the distinguishing analytes by ionization characteristics. As shown in Figure 2.2, a PID-type sensor consists of ultraviolet (UV) source to excite diffused VOC molecules for ionization and two electrodes which provide the circulation of formed ions.[31,35,38] This current flow is then converted into sensor signal which corresponds to gas concentration. Main drawback of PID-type sensors is the non-selectivity since they have potential to ionize any compound with an ionization energy less then UV source.[31] It must be used with a gas chromatography device (GC-PID) in order to distinguish selective VOCs.[38]

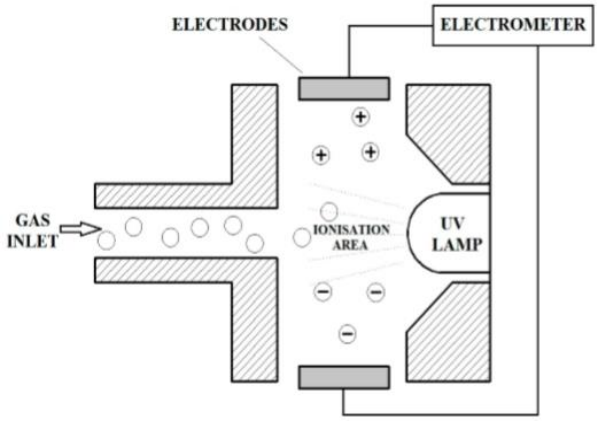

Figure 2.2 Schematic illustration of photoionization detector (PID-type) sensor.[31]

One of the most viable sensors for in-situ measurements is resistive-based gas sensors consist of metal oxide, which also called semiconductor metal oxide sensors (MOx or MOS). The sensing mechanism of these sensors relies on the change in the sensor resistance or conductivity upon exposure to the analyte.[27,35] The sensor system consists of a receptor surface (which is metal oxides such as SnO_2 , ZnO, Al_2O_3, etc.) with electrodes (Pt or Au) and, a heater to optimize the temperature of the receptor layer (Figure 2.3).[27] When the ambient air interacts with the semiconducting materials, chemisorption of oxygen molecules occurs and causes an increase in the electron depletion layer and so resistance. After the exposure of VOCs which have a reducing nature, gas molecules react with oxygen ions and release the trapped electrons. Eventually, the electron depletion layer decreases, and thus VOCs are detected from the change in the electrical resistance of the sensing layer. [27,30,31,35] The metal oxide-based sensors are attractive for VOC sensing due to their high potential of integration in portable devices and the high sensitivity.[39–41] But yet it is a complicated process which consists of diffusion, chemisorption and desorption of gas molecules, and reduction/oxidation processes. The disadvantageous of MOx sensors are the long recovery times, poor stability, and high energy consumption due to the requirement of high temperature (500–900 K) for the reactions.

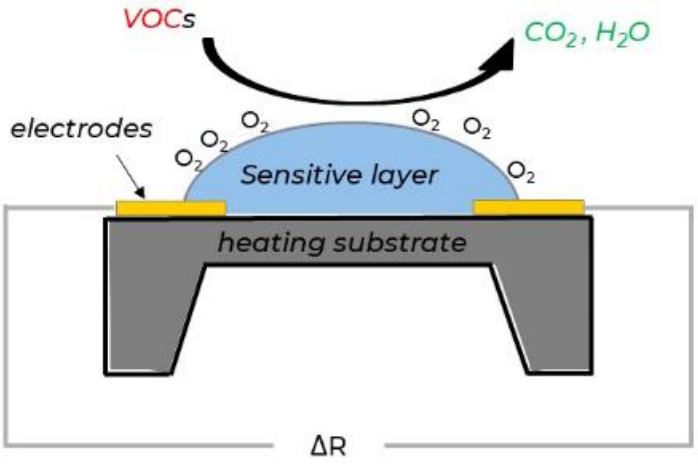

Figure 2.3 Schematic illustration of the operation principle of resistive-based sensor.

Among these techniques, although miniaturization of the sensors was successfully accomplished via micro- and nanoscale manufacturing methods to a scale that can be integrated to the portable (or wearable) devices, the manufacturing methods usually involves multiple steps that contributes to the cost, and complexity to the operation. Besides, it has also been stated that the current methods also involve operation issues in continuous monitoring such as reliability, precision, selectivity, and stability.[30,35] Thus, improvement of the sensor that is targeted toward affordability and ease of operation is desired for broader use of such sensors.

Optical sensors have attracted attention as an alternative to commercial electronic sensors since they offer rapid, sensitive, and energy-efficient in-situ detection. The working principle is the changes in the light properties such as wavelength, amplitude, intensity, and polarization state of the light for optical sensors.[29,42,43] In literature, optical fibers[29,44–46], co-polymers[47,48] and composites[49–51] are the materials that have been used in the colorimetric sensing of VOCs. The sensing mechanism of these sensors is based on the utilization of the molecular interaction between the target analyte and the sensing element.[52] These interactions result in the change in the refractive index, absorbance or reflectance spectra, reflected wavelength of the sensing material by the alteration of polymeric layer thickness, size, shape and assembly of the nanoparticles, intermolecular or interparticle distances.[30,52,53]

Besides these materials, liquid crystals (LCs) also offer high sensitivity by the contribution of their elastic properties.[54,55]

Previous studies have demonstrated that the optical response of LC-based sensors upon exposure to VOCs arises from the molecular reorganization of LCs, resulting in either a phase transition or an orientational transition. Typically, these systems involve an LC layer supported on a functionalized solid surface to provide a preferred orientation of LC molecules. In a recent study demonstrated the advantage of elastic energy in the VOC-induced orientational transition results in an apparent optical change of the nematic LC (5CB) films.[55] They obtained elastically strained LC films by confining the nematic LC in chemically patterned microwells that impose planar alignment at bottom glass substrates (functionalized by either gold or polystyrene) while free interface induces homeotropic alignment. This confinement causes an energy penalty due to the deviation of director from easy axis orientation at the bottom interface of microwells and thus introduced a strain to anchored LC. Figure 2.4A reveals that toluene-triggered optical change of 5CB film recorded at different pressures of toluene vapor. Ultimately, toluene vapor allows the director to relax by decreasing the anchoring strength and enables uniform homeotropic alignment (strain-free state) at 1520 mTorr of toluene vapor (the right image of Figure 2.4A). This optical response of the 5CB film is consistent with a decrease in the optical retardance with the increasing of toluene pressure, as shown in Figure 2.4B. The experiments also established that the higher surface roughness and thinner films required lower energy to induce the orientational transition of LC films (Figure 2.4C).

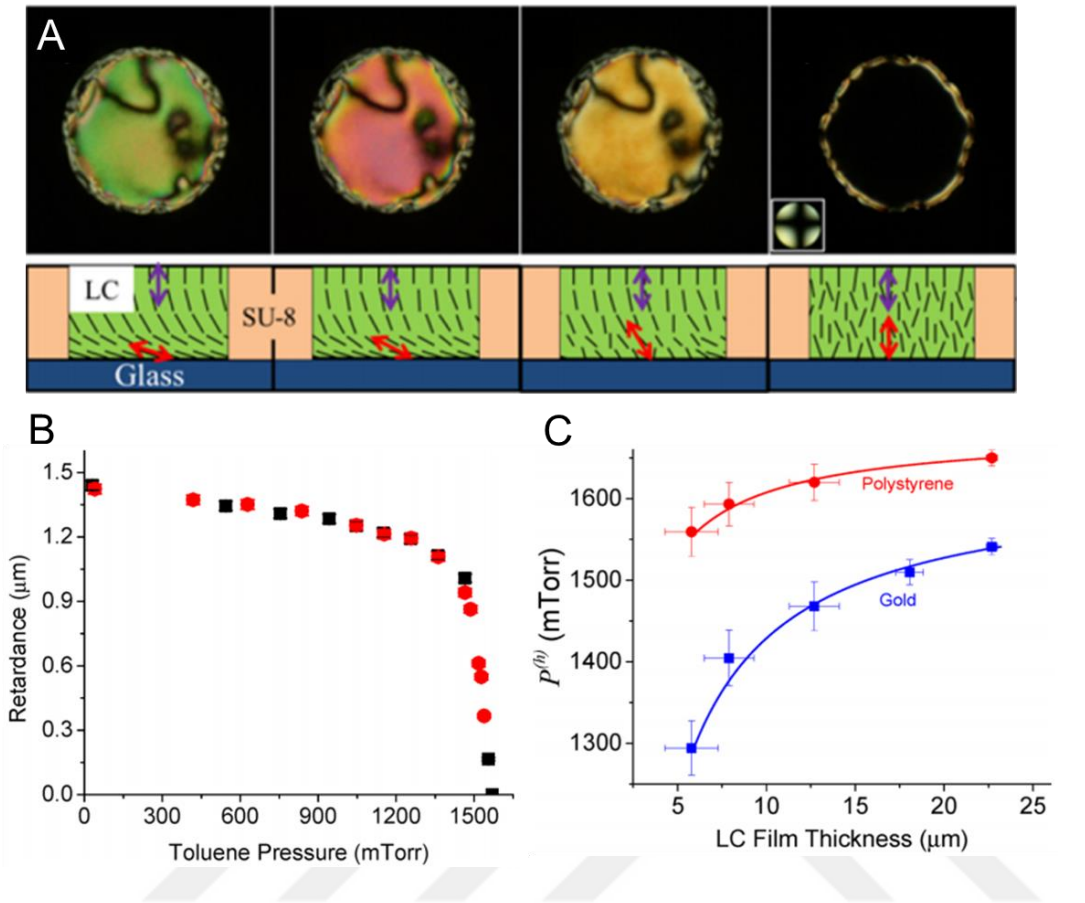

Figure 2.4 (A) Optical images of 5CB exposed to different vapor pressures of toluene: from left to right, 0 mTorr, 1410 mTorr, 1520 mTorr, and 1570 mTorr, respectively. The arrows represent the director orientation at the LC-air (purple) and LC-glass (red) interfaces. The dimension of microwells is 200 μm in diamater and 14.9 μm in thickness. (B) Retardance measurement of 5CB film as a function of toluene pressure. Black squares represent data obtained as toluene pressure increased. Red circles represent data obtained as the toluene pressure decreased. (C) Measured responses of films of 5CB upon toluene exposure when supported on either polystyrene (red circles) or gold (blue squares) substrates.[55]

Metal-cations (e.g., Cu^{2+} or Al^{3+}) deposited solid surfaces are commonly used functionalized surfaces for gas sensing. The homeotropic orientation of the nitrile-containing LCs (such as 5CB or E7) on such surfaces due to the molecular interactions between the metal-cations and nitrile group was previously reported.[56] The adsorption of a gas analyte on the metal-salt functionalized surface might trigger the orientational transition of LC from homeotropic to planar alignment due to the competition of molecular interaction between the analyte and LC molecules (Figure

2.5A).[24,54,56] In such a study, Nayani et al.[54] synthesized a new nitrile-based LC mixture (PCH3/PCH5) that exhibit a planar alignment at the LC-air interface (left scheme of Figure 2.5B), in contrast to commercial nitrile-containing LCs such as 5CB (left scheme of Figure 2.5A). The authors aimed to create an initially strained platform by this hybrid alignment (planar at a free surface to the atmosphere and homeotropic at the La^{3+} perchlorate functionalized surface) and thus to improve the response and sensitivity of the sensor due to the stored elastic energy in strain state of the LC. After the introduction of dimethyl methyl phosphonate (DMMP) as a vapor to both the strain-free (5CB) and the strained state (PCH3/PCH5) LC system, molecular reorientation was quantified by measuring the intensity of transmitted light through the LC system. Figure 2.5C demonstrates that the elastically strained, hybrid alignment exhibits faster response and greater sensitivity upon exposure to DMMP vapor, when compared to the 5CB case. This improved properties of hybrid system arise from the relaxation of the LC director with a release of initially stored elastic energy in LC film.

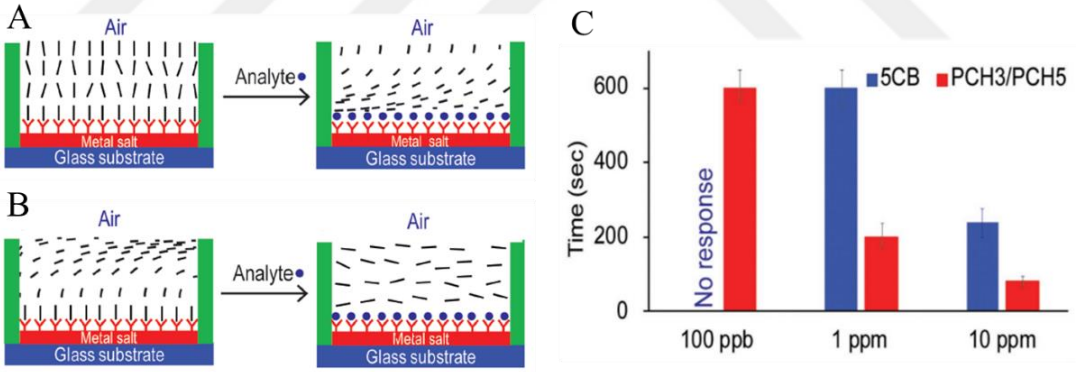

Figure 2.5 (A) Schematic representation of director profile of 5CB supported on a La^{3+} decorated surface with homeotropic anchoring at the free surface, prior (left) and after (right) the dimethyl methyl phosphonate (DMMP) exposure. (B) Director profile of PCH3/PCH5 mixture supported on a metal-salt-decorated surface and a planar anchoring at the free interface, prior (left) and after (right) the DMMP exposure. (C) Characteristic time to achieve an 80% response for PCH3/PCH5 and 5CB as a function of DMMP concentration.[54]

LCs confined in polymer fibers have also been used as alternative gas sensing platforms that offer flexibility and porosity besides low-cost and simple production.[57–59] For example, Lagerwall et al. developed nonwoven mats of electrospun fibers comprised of a nematic LC (5CB) core covered by poly(vinylpyrrolidone) (PVP) sheath.[57] Figure 2.6 demonstrates the reversible optical response of uniformly aligned fibers upon exposure to toluene vapor. Reduction in the brightness of PVP-LC fibers during the exposure is observable both with the naked eye and between crossed polarizers. The mechanism underlying this response is the rapid loss of defined orientation due to the incorporation of toluene vapor through the polymer sheath into 5CB, thus removing the twist that procured from the cylindrical confinement.

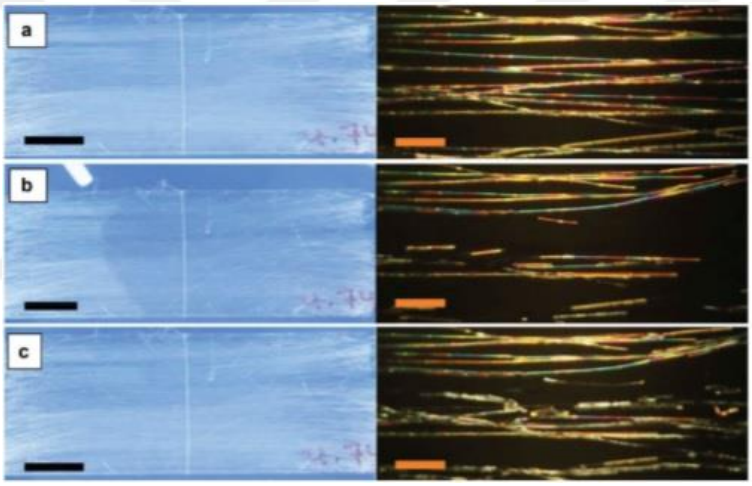

Figure 2.6 Aligned mat with coaxially spun PVP-LC fibers (a) before, (b) during and (c) after toluene exposure, as observed macroscopically between crossed polarisers (left column; scale bars: 10 mm) and through the POM (right column; scale bars: 80 μm), respectively.[57]

A recent study of Guan et al. has taken LC-functionalized fibers a step further and turned them into wearable sensors without any power supply.[59] They produced a nylon fiber clad by a cholesteric liquid crystal (CLC) mixture and stabilized the cladding with polymer (PVP) sheath (Figure 2.7A). Figure 2.7B shows the red-shift of the fibers woven into a fabric with combine colors during heating. The authors have not conducted any experiment of woven fibers upon VOCs exposure, yet, they

have shown the potential to be employed as wearable gas sensors in textiles. The incorporation of CLC in this study provided the advantages of both the color variation over a certain temperature range and the fact that the presence of different external stimuli, such as temperature variation, can change the helical pitch, thus leads to a shift of the selective reflection band which is observable with the naked eye.

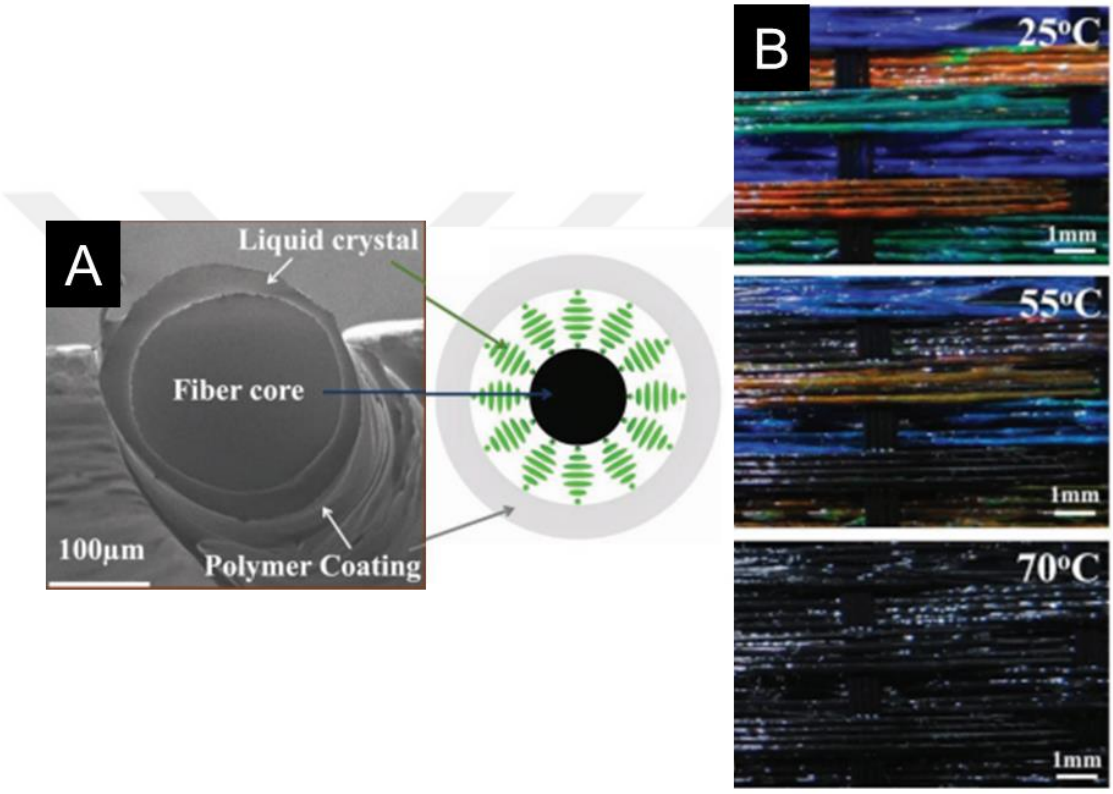

Figure 2.7 (A) SEM image of a 200 µm diameter nylon fiber clad with a CLC mixture (cholesteryl nonanoate:cholesteryl oleyl carbonate:cholesteryl chloride = 1:1:0.6) and stabilized with a PVP outer sheath. And the schematic illustration of the cross-section of the coated fiber showing the helical structure of the CLC director. (B) The optical change of the CLC-clad fibers woven into textiles during thermal treatment.[59]

In our study, cholesteric liquid crystals (CLCs) were employed in order to develop an optical sensor. There have been several attempts to use CLCs as VOC sensors.[20,22,43,60–63] Winterbottom et al. described preliminary studies of CLC sensors for the sensing of organic vapors.[62] In this study, the responses of CLC films, which

were cast from the binary mixture of cholesteryl esters on a glass substrate, were analyzed upon the exposure to acetone, pyridine, benzene and hexane. After placing the CLC films in an air-closed vessel containing 1.0 ml of organic vapor, reflectance spectra were recorded by using a spectrophotometer. Spectrum results showed that while benzene and hexane gave a colorless shift, acetone and pyridine caused a slight red-shift of the reflection band. In addition, the effect of the composition of CLC films on the sensitivity and selectivity of the sensor was demonstrated. The main drawback of this study is the poor stability of CLC films. The authors were tried to overcome this crystallization issue by immobilizing the CLC films in a polymer network. However, the results were not clearly and deeply discussed.

In another study, the mass-sensitive and optical methods were successfully combined to investigate the sensitivity of a CLC sensor in the detection of different organic vapors.[20] Mujahid et al. prepared the CLC coatings from a chiral biphenyls mixture and tested them upon exposure to some polar (ethanol and methanol) and non-polar organic vapors (tetrahydrofuran (THF), chloroform and tetrachloroethylene). The changes of the optical properties were recorded by using a spectrophotometer and a blue-shift of the absorbance band was observed. Figure 2.8 demonstrate the linear relationship between the absorbance shift (ΔA) and the molar mass of the analyte. The authors also stated that the less polar solvents lead to a larger shift on the absorbance band due to stronger interactions with the LC than polar solvents. Lastly, they prepared a CLC dispersed polystyrene network to provide robust and mechanically stable material. Combining CLCs with imprinted polymers also led to a significant increase in the sensor selectivity compared to pure CLC material.

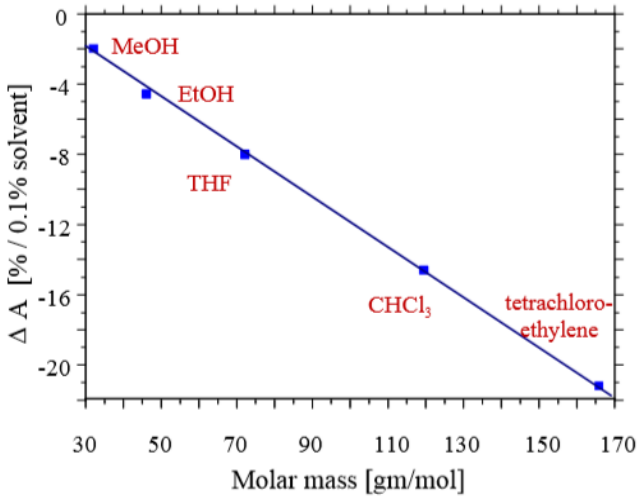

Figure 2.8 Optical sensor response of CLCs towards molar masses of different analyte vapours.[20]

Molecular imprinting is a useful method to improve the selectivity and sensitivity of the CLC sensors since the porous and template oriented materials favor the sorption of target solvent vapors. In such a study, hydrogen-bridged CLC polymer networks were used as optical sensors to distinguish methanol from ethanol in synthetic wines.[23] They prepared CLC mixtures by using different compositions of reactive and non-reactive mesogens, chiral dopant, and alkyloxybenzoic acids. After the photo-polymerization of CLC mixtures as hydrogen-bridged CLC films, porosity was created by the extraction of the non-reactive LC mesogen (Figure 2.9A). In this way, they aimed to detect alcohol molecules according to the difference in their molecular affinity with carboxylic groups of the cholesteric network and to improve sensitivity due to increased surface to volume ratio. Figure 2.9B shows the transmission wavelength of the CLC films increased upon the absorption of alcohol solution with a higher concentration of ethanol since the ionic interaction of ethanol is larger than methanol with hydrogen-bridged CLC polymer. Furthermore, they observed that the sensitivity was improved by increasing the alkyloxybenzoic acid content and decreasing the cross-link density in the polymer network.

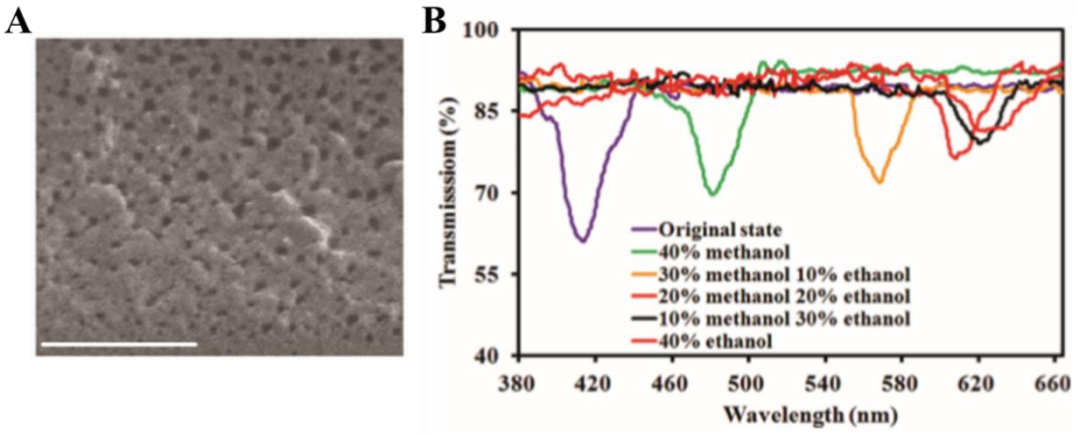

Figure 2.9 (A) The scanning electron micrograph (SEM) of the CLC film after the extraction of 5CB. Scale bar: 2 μm. (B) Optical transmission spectra of CLC in alcohol solutions with different ratios of methanol/ethanol.[23]

On one of the recent studies of Kek *et al.* presented the relationship between the molecular structures of CLCs and the shift in their reflection spectrum upon the exposure to different VOCs. They prepared seven CLC mixtures by adjusting the contents of nematic LCs and chiral dopants. Green reflected CLC films (~550 nm) were obtained by spin-coating this mixtures on a glass substrate. As shown in Figure 2.10A, CLC films were placed in a small container, VOCs were introduced as 5 μL by using a micropipette, and the wavelength shift of the selective reflection was recorded by using a spectrophotometer. They investigated the factors to control the direction and the magnitude of color shift depending on the structure of CLCs such as bulky substituents, hydrogen bonding, and elastic constants. Figure 2.10B shows the red-shifted reflection spectra of a CLC mixture of NmLC (6) [E-7] which are composed of biphenyl and terphenyl derivatives, doped with the same chiral dopants upon interaction with methyl ethyl ketone (MEK), toluene, cyclohexane or tert-butyl alcohol. This result was supported by optical images of the CLC film before and after exposure to toluene vapor (Figure 2.10C). Although a response is observed, this study had several bottlenecks. First, a CLC was used in the liquid form that would be hard to stabilize in practical use. Second, they have used a spectrometer to determine coloring of the films, which adds cost to the sensor. Third and more

importantly, they reported optical response upon toluene exposure at concentrations close to the saturation concentrations of toluene at ambient temperature that is beyond the permitted exposure limits (in the order of 100 ppm).

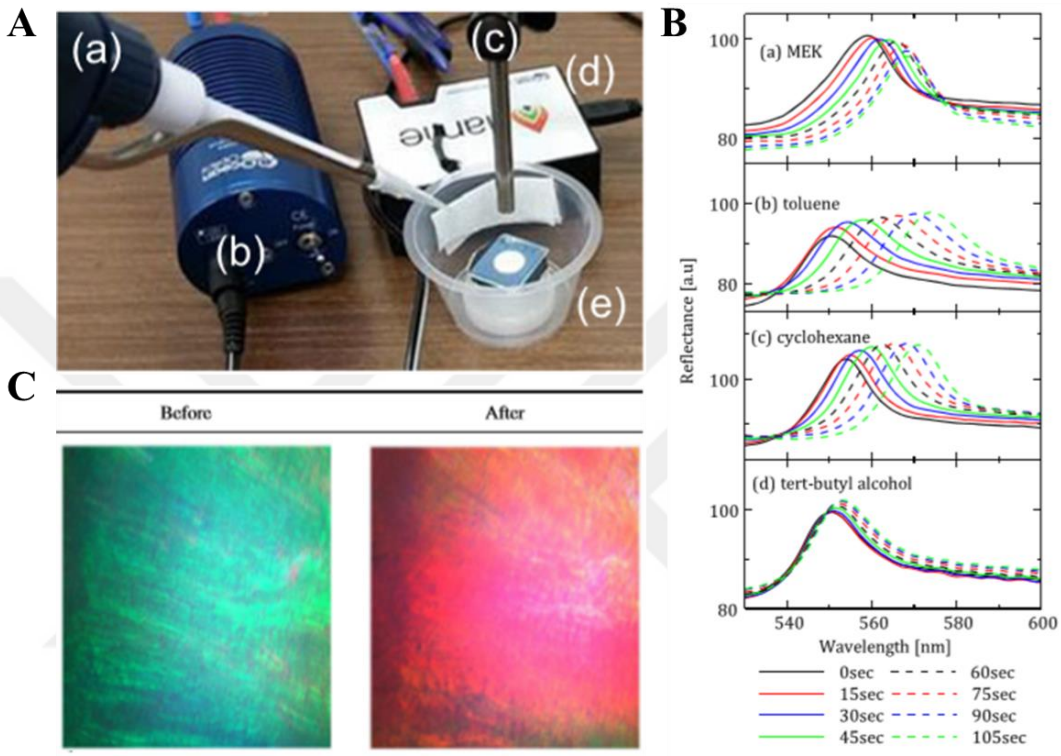

Figure 2.10 (A) Experimental setup to measure selective reflection spectra; (a) micropipette, (b) halogen lamp, (c) optical probe, (d) spectrophotometer, (e) sample. (B) Optical images of the sample before and after exposure to toluene vapors (C) Time-lapsed reflection spectra of CLC mixture of nematic LC (E7) and chiral dopant (mixture of DDS-1015L/NYC-22133L) upon contact with 5 µL of (a) MEK, (b) toluene, (c) cyclohexane and (d) tert-butyl alcohol.[43]

All these past studies have shown that the sensor durability, response, and sensitivity to external stimuli could be improved significantly by polymerization of the sensing LC platform. There are various procedures for the synthesis of polymeric materials that retain the self-organization of liquid crystals (LCs) while ensure a robust structure. For example, polymer-stabilized LCs and polymer dispersed liquid crystals (PDLCs) are obtained from the polymerization of nonmesogenic reactive monomers with nonreactive LC mesogen. Differently from this, polymerization of

reactive mesogens, which comprise functional monoacrylate or diacrylate substitutes, results in the liquid crystal elastomers (LCEs). Cholesteric LC elastomers (CLCEs) combine the significant mechanical properties of elastomers with the unique optical properties provided by the inherent helical structure of CLC molecules. Thus, make them a perfect candidate for colorimetric sensor applications that respond to external stimuli such as strain, temperature, pH or humidity. Polymerization of mixtures of reactive and nonreactive mesogens were also provided by different studies.[14,64–66] In such a study, Karausta and Bukusoglu synthesized porous polymeric films templated from nematic LCs to be employed as ultrafiltration membranes.[64] Following the procedure of photo-polymerization of a mixture of non-reactive (5CB) and the reactive (RM257) mesogen between two functionalized glass substrates (rubbed-PVA surfaces for the planar alignment, perfluorodecyltriethoxysilane (PFDTS)-deposited surfaces for the homeotropic alignment), the extraction of non-reactive mesogen, result in a director-dependent shrinkage of obtained films while maintaining LC configuration. Optical microscope images prove that the LC alignment within the film was retained both before and after the extraction step. As shown in Figure 2.11A, polymeric films with planar anchoring exhibited dark appearance under polarized light since the LC alignment was in the direction of one of the polarizers while the bright appearance was obtained when the film was rotated 45°. Moreover, higher shrinkage was achieved in the perpendicular direction of LC anchoring. Compatible with these results, the films with homeotropic anchoring exhibited isotropic shrinkage and their appearance did not change under polarized light. This developed method provides control over the polymer chain alignment and thus the pore alignment through predetermined LC orientation.

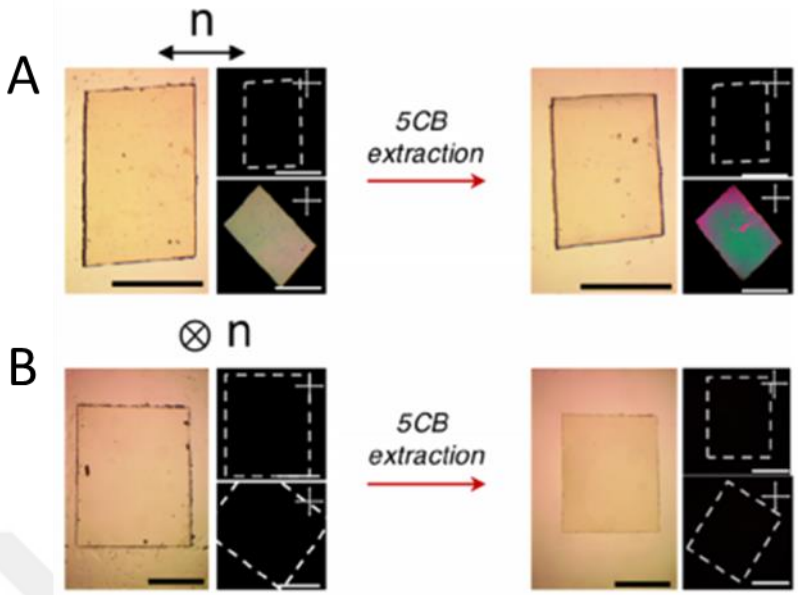

Figure 2.11 Brightfield and polarized optical micrographs of of 40 μm polymeric films synthesized from mixtures of 20% RM257 and 80% wt. 5CB. (A) Planar anchoring, and (B) homeotropic anchoring are demonstrated before (left images) and after (right images) extraction of 5CB. 'n' indicates the nematic director. Crossed lines in figures indicate the direction of the polarization of the polarizer and analyzer. Dashed lines in the images were drawn to indicate the boundaries of the films; scale bar: 500 μm.[64]

More recently, combination of the photolithography method with LC molecular templates described above was demonstrated to provide microparticles with various shapes while controlling the LC configuration within them.[65,67]

All these past studies either have stability issues due to the use of LC in a liquid form or have not performed any sensitivity measurements of their sensors for the low exposure limits of VOCs which determined by authorities. Herein we aimed to go beyond these past studies and monitor VOCs only from a visible optical appearance at a determined concentration range as low as 100 ppm. For this purpose, we use CLCs to template the polymerization of particles that demonstrate structural coloring through Bragg reflections. We expect to provide statistical data on the response of polymeric particles and durable sensors for long term use.

CHAPTER 3

MATERIALS AND EXPERIMENTAL SECTION

3.1 Materials

Nonreactive LC mixture E7 (mixture of 51% of 4-cyano-4'-pentylbiphenyl (5CB), 25% of 4′-heptyl-4-biphenylcarbonitrile (7CB), 16% of 4′-n-octyloxy-4-cyanobiphenyl (8OCB) and 8% of 4-cyano-4"-n-pentyl-terphenyl (5CT)), and reactive monomer 4-(3-acryloyoxy-propyloxy)benzoic acid 2-methyl-1,4-phenylene ester (RM257); chiral dopant 4-(1-methylheptyloxycarbonyl)phenyl-4-hexyloxybenzoate)) (S-811) (Jiangsu Hecheng Chemical Materials Co. Ltd.); polyvinyl alcohol (PVA), 3-(trichlorosilyl)propyl methacrylate (TCSPM), photoinitiator (2,2 dimethoxy-2-phenylacetophenone) (DMPAP), anhydrous acetone and toluene (Sigma-Aldrich Co. Ltd.); anhydrous ethanol (J.T. Baker Co. Ltd.) were used without further treatment. Glass slides and cover glasses were obtained from Marienfeld GmbH. The lithography mask consisted of the circle shapes with 100 μm diameter. The PVA mold consisted of the circle shape microwells with 100 and 7 μm diameter, and 8 μm depth.

3.2 Preparation of the Monomeric CLC Mixtures

Mesogen mixture (100 mg) consisting of 20 wt % RM257, 72 wt % E7, 8 wt % chiral dopant and 1 wt % photoinitiator (See Figure 3.1A for molecular structures) was dissolved in toluene in a 1:0.5 ratio to form a homogeneous solution. The solvent was then evaporated under vacuum to obtain homogenous cholesteric liquid crystalline mixture. The ratio of chiral dopant was changed depending on the desired color of polymeric particles.

3.3 Preparation of the Glass Surfaces

Glass slides and cover glasses were coated with 5 wt % PVA aqueous solution, to induce a planar anchoring of LC molecules. Glass substrates were spin coated with PVA at 5000 rpm for 2 minutes and rubbed with a velvet cloth to maintain planar alignment of LCs. In order to covalently bond the particles to the glass surface, TCSPM coating was carried out. Firstly, oxygen plasma was applied to the glass surfaces using a Diener Electronics, Zepto Plasma Unit. Then, glass surfaces and 75 μL of TCSPM were placed inside the desiccator and incubated overnight under vacuum. Treated glasses were then rinsed with absolute ethanol and dried with nitrogen gas.

3.4 Preparation of CLC Templated Polymeric Particles

In mask lithography method, the monomeric CLC mixtures were polymerized in a sandwich cell prepared with two coated (PVA or TCSPM) glass surfaces. The thicknesses of the particles were set by using a polyethylene film as a spacer. The CLC mixture was then filled in a sandwich cell with 20 μm spacer at room temperature using capillary action followed by photopolymerization under a collimated 365 nm UV light source (ThorLabs M365LP1-C1). The shape of the particles was provided by using a desired shape and size photomask which placed just above (no gap) the sandwich cell. Exposure times were varied from 1 to 5 s depending on the set power, which was varied in the range 1−2.5 mW cm^{-2} at a distance of 3 cm from the light source. Here we observed that the long exposure time of the UV light led to complete polymerization of the mixture resulting in the formation of a film. Thus, determining the optimum exposure time is critical in determining the initial shapes of the particles. After polymerization, the glasses were detached by treating with absolute ethanol inside a beaker to obtain a free standing polymeric particles. The resulting particles were then centrifuged at 5000 rpm for 5 mins for the extraction of nonreactive mesogen. The centrifugation was repeated for

at least three times as a cycle of precipitation and replacing the supernatant with fresh ethanol. Then, the templated particles were collected and dried at room temperature for further analysis. The procedure can be followed in Figure 3.1B.

In soft lithography method, polymerization of the CLC mixtures were performed in sacrificial PVA molds consisting of either 7 or 100 μm-in-diameter circular microwells with 8 μm depth. We used an uncollimated 365 nm UV light source (Spectroline ENF-280 C/FE) that delivered 2.5 mW cm^{-2} at a distance of 5 cm away from the light source. Microwells were exposed to UV light for 30 min. Particles were readily obtained by dissolving the PVA mold in distilled water and then extracted with the same procedure performed in the mask lithography (Figure 3.1C).

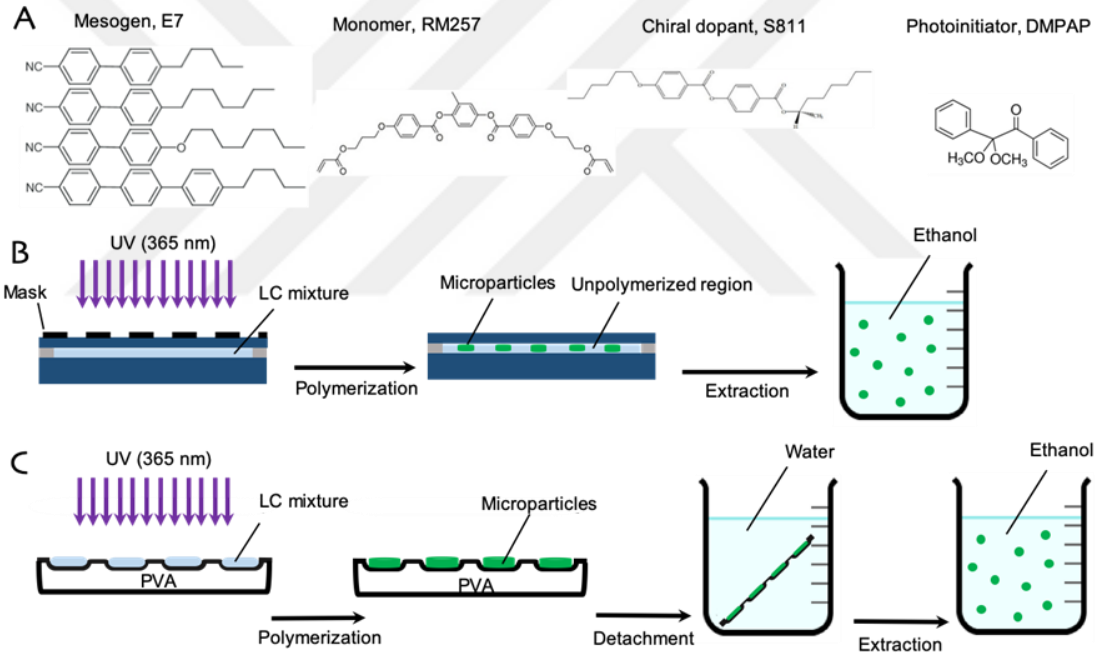

Figure 3.1 (A) The molecular structures of the reactive, non-reactive mesogens, chiral dopant and photo initiator. Schematic illustration of the experimental methods for the synthesis of particles using (B) photolithography and (C) soft lithography.

3.5 Optical Characterization and Measurements

We performed optical characterizations of the particles by using an Olympus BX53 microscope (Japan) equipped with 4x, 10x, 50x, and 100x objectives and crossed

polarizers. The bright field (BF) and polarized (PL) micrographs were collected in transmission and reflection modes. We analyzed the images by an open source image analysis software, Fiji ImageJ.

3.6 Response Measurements

For the sensor test, we installed a vacuum system that allows introducing certain concentrations of solvent vapor at 100 ppm intervals while monitoring the optical appearance of the particles. The experimental setup consisted of a toluene reservoir, a series of valves for introducing and adjusting the concentration of toluene, and a vacuum pump is illustrated in Figure 3.2. Specifically, a glass window of the exposure chamber enables us to acquire online images of the samples through an optical microscope. The sensor tests were carried out at room temperature between 0 ppm to saturation vapor pressure of toluene. Before each test, the system was evacuated to 0.08 torr using a vacuum pump. Then, the toluene concentration delivered to the system is controlled by pressure values using the Baratron® capacitance manometer (MKS Instruments). At each desired concentration, we allow the system to equilibrate for at least 3 minutes and then we collected images in the reflection mode of a polarized optical microscope. Before starting the sensor tests, the toluene reservoir was placed in liquid nitrogen and degassed by the freeze-pump-thaw technique. Then, we quantified the red-green-blue (RGB) values of each micrograph with the Fiji ImageJ program and obtained response curves that demonstrate the signal change with respect to increasing toluene concentration or with respect to time. The normalized signal is shown in Equation 4.

$$signal = \left(\frac{\left(\frac{R}{G}\right) - \left(\frac{R}{G}\right)_0}{\left(\frac{R}{G}\right)_0} \right) \qquad \text{Equation 4}$$

where R, G, and B are the average intensities of measured red, green, blue signals and the subscript zero indicates corresponding value at 0 ppm of toluene.

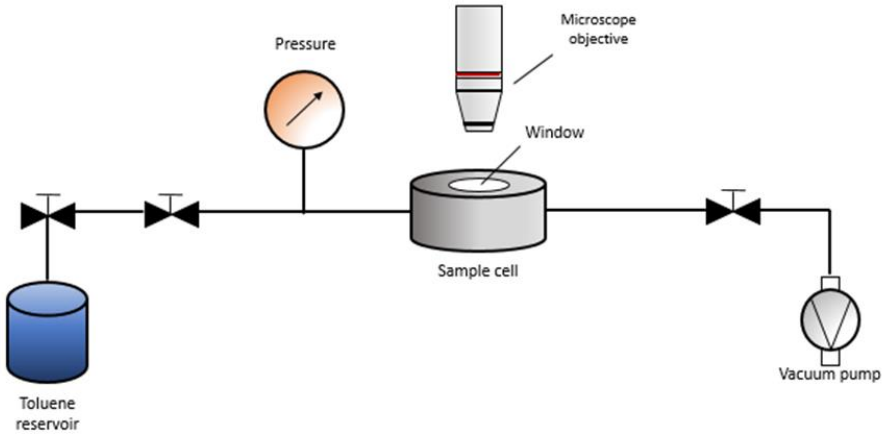

Figure 3.2 Schematic representation of the experimental setup used for exposure the CLC templated polymeric particles to toluene vapor.

CHAPTER 4

RESULTS AND DISCUSSION

Before investigating the optical responses of CLC-templated polymeric particles triggered by VOC vapor, we first performed their characterizations. Our initial interest in this part of the study was to understand the optical appearance and the internal structure of the particles to be used as sensors to interpret the origin of the response of the particles against VOC vapor. Thus, the results that we report herein first describe the characterizations of the particles, then continues with the sensor tests and response characteristics of the particles upon VOC exposure. Lastly, we present the results that show the reliability and durability of the sensors prepared in a chip form that is motivated for real-time applications.

4.1 Synthesis and Characterization of Cholesteric Liquid Crystal Templated Polymeric Particles

We synthesized CLC templated polymeric particles following mask lithography and soft lithography procedures described in Figure 3.1 B and C and synthesized particles of sizes 7 and 100 μm. We chose such two different sized particles that provided us insight into the response of the particles that we describe below. Figure 4.1 shows the optical micrographs collected during the synthesis of the particles. The images include micrographs taken before polymerization, after polymerization and after extraction of the unreacted mesogens. The micrographs shown in Figure 4.1 are categorized into three sections; 100 μm-sized particles synthesized by mask lithography (Figure 4.1A), 100 μm-sized particles synthesized by soft lithography (Figure 4.1B), and 7 μm-sized particles synthesized by soft lithography (Figure 4.1C). In all cases, CLC mixture contained 20% wt RM257 and 8% wt chiral dopant in E7 to provide Bragg reflections in the visible wavelengths. As shown in column

(i) and (ii) of each three cases, the Bragg reflections from the particles were not visible either before or after polymerization as evidenced by these reflection-mode polarized optical micrographs. After extraction of the unreacted mesogens, particles shrank (both along the cylindrical axis and radial direction) and the pitch size decreased, and this shrinkage led to a pitch that allow reflection within the visible wavelengths as shown in column (i). We note that we have followed critical steps in the synthesis not to deform the particles as the deformation may affect the optical appearance of the particles. Details of such procedures can be found elsewhere.[65]

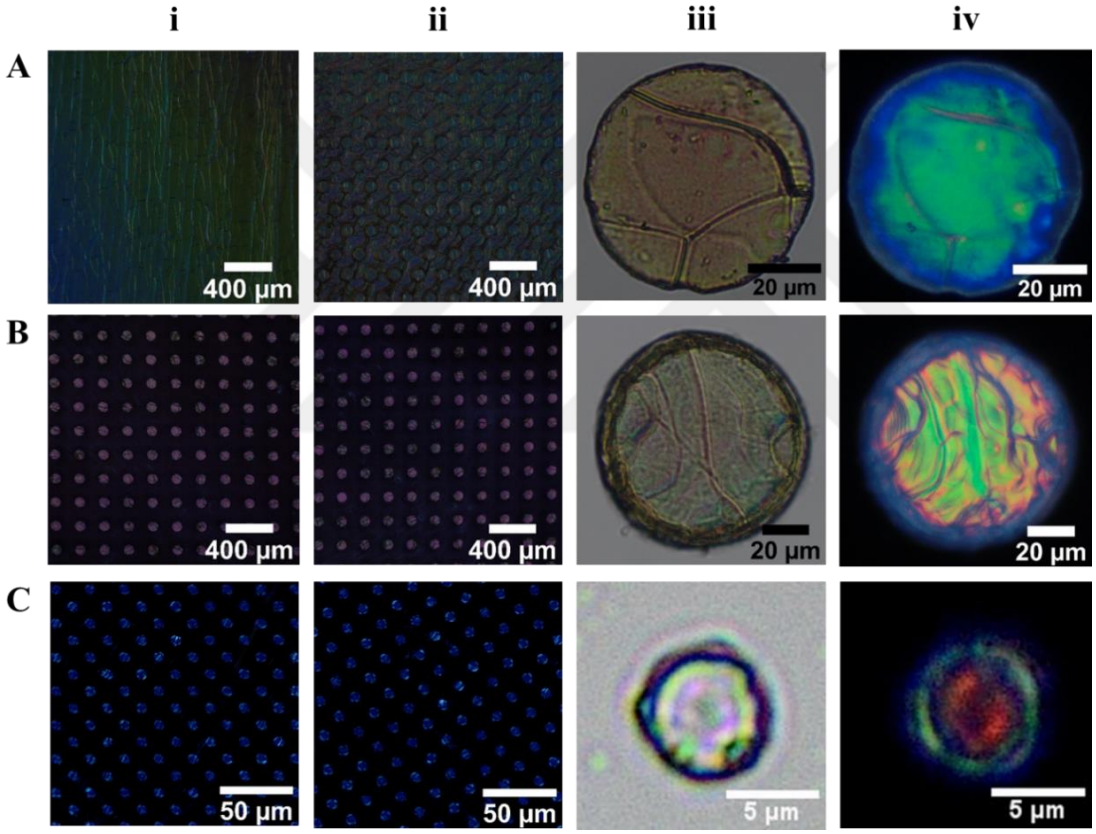

Figure 4.1 Optical micrographs collected during the synthesis of polymeric particles from a mixture of 20% RM257, 72% E7, and 8% wt S811. (A) 100 µm particles synthesized by mask lithography, (B) 100 µm and (C) 7 µm particles synthesized by soft lithography. The column (i) of each method contains images of before and (ii) after polymerization (bottom row), the other two columns of each method show micrographs of produced particles after extraction in (iii) bright field and in (iv) reflection mode of microscope.

In order to provide structural colors in the desired visible wavelength, we prepared mixtures of different chiral contents in the range of 0.3-10 % wt. and synthesized 100μm particles within microwells. Figure 4.2A shows that particles possess structural colors in a certain range of chiral content of the mixture, any chiral content above or below this region brings Bragg reflection in the invisible region of light. Also, in this visible range, we observed color changes from longer to shorter wavelengths (blue shifted) with decreasing in the pitch size of the helical structure due to increasing of chiral content (Equation 2). Then, we analyzed the shrinkage behavior from size measurements on the micrographs of the particles before and after extraction. We obtained ~10% shrinkage in the radial direction for all cases (Figure 4.2B), which means once the helical structure obtained, particles exhibit the same behavior during extraction. This result is similar to the shrinkage amounts that are observed parallel to the director in nematic LC particles (or films).[64,65] Due to the three-dimensional confinement of the cholesteric phase within the microwells, the shrinkage amounts observed after extraction in the radial direction was similar to the shrinkage amount observed in nematic films, parallel to the director.

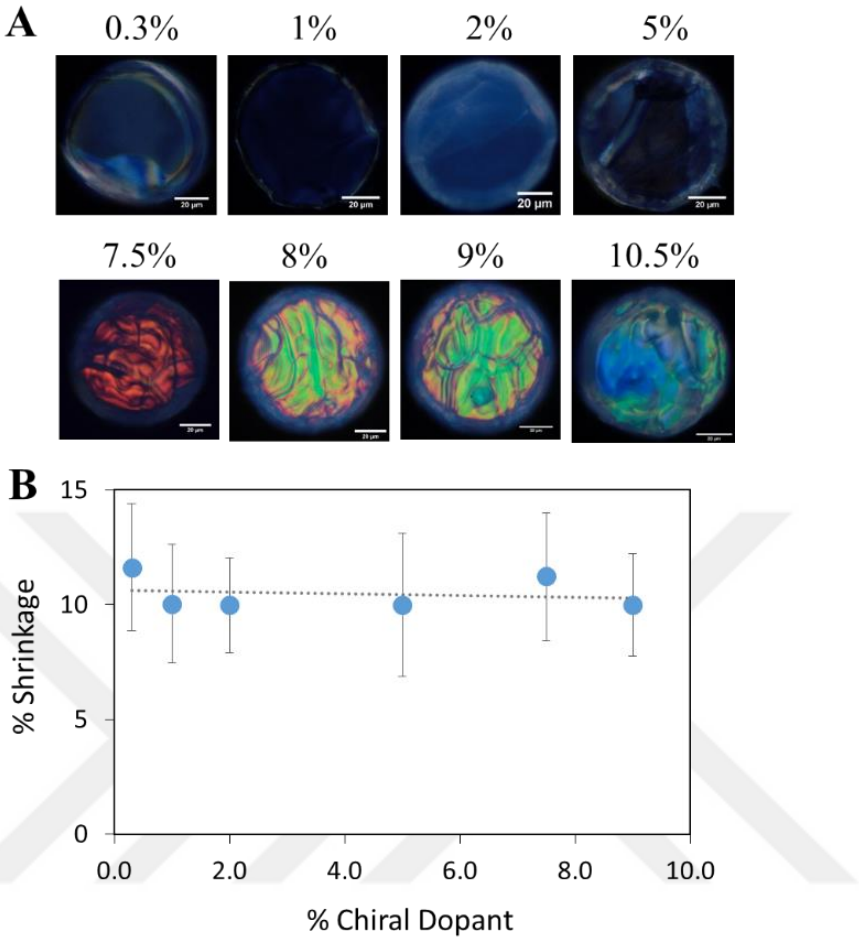

Figure 4.2 (A) Reflection mode polarized micrographs of the particles synthesized from mixtures containing 20% wt RM257 and balance E7. (B) Plot of shrinkage observed after extraction of the unreacted mesogens as a function of the chiral dopant concentration. Scale bars: 20μm.

After the synthesis of particles with the desired color, we performed characterizations on particles of same size (100 μm) that were produced by different methods, and particles with different sizes (100 μm and 7 μm) that were produced by the same method to understand the effects of the synthesis method and the size, independently. As shown in part (iv) of Figure 4.1A and B, we observed a difference in color hue of green reflected particles between two methods although we used the same synthesis mixture (20% wt. RM257 and 8% wt. chiral dopant in E7). In the control experiment to explain this color hue difference, we prepared two groups of

sandwich cells using the same mixture and produced polymeric films with two different polymerization times as 3 seconds and 30 minutes. Figure 4.3 shows the comparison of these films produced by different methods. We observed the color similarity of the film polymerized for 30 minutes with the soft lithography particles and the film polymerized for 3 seconds with the mask lithography particles. It can be explained simply by our previous observation that the two different synthesis methods provide different polymerization degrees due to the differences in UV exposure times for polymerization.[64,65]

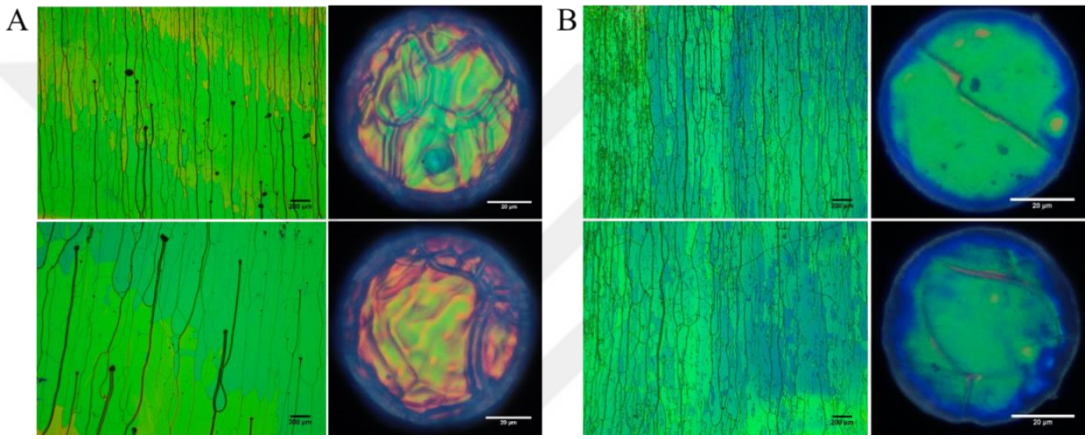

Figure 4.3 Reflection-mode polarized optical micrographs of polymeric films taken after extraction and color comparison with polymeric particles. (A) The film polymerized for 3 sec and (B) for 30 min.

On the other hand, when we compared the appearances of the 100 μm (Figure 4.1B) and 7 μm (Figure 4.1C) sized particles synthesized by the soft lithography method, we observed the small sized particles to maintain a red color corresponding to a higher wavelength compared to that of the 100 μm-sized counterparts. We attribute this difference to result from the initial configuration maintained within the microwells. When the particles were synthesized within microwells, the alignment of LCs were homeotropic at the top side open to air whereas they were planar at the sides contacting PVA surfaces. Due to this three-dimensional confinement, the shrinkage of the particles was affected by their surfaces when the particles were smaller in size. Since we have shown in our previous studies that the particles shrink more in the direction perpendicular to the individual director of the particles,[64,65]

such three-dimensional confinement would result in a lower shrinkage of small particles compared to their larger counterparts. In order to provide further support to this observation, we determined the percent shrinkage values from size measurements on the micrographs of the particles before and after extraction. These measurements revealed 10.5 ± 1.8% and 7.7 ± 2.7% shrinkage in the radial direction for 100 μm and 7 μm particles produced by soft lithography, respectively, consistent with our hypothesis (Figure 4.4A). We also note that we are more interested in shrinkage in the direction of the cylindrical axis since it gives information about the change of the pitch size perpendicular to the imaging direction. We have estimated such shrinkage as ~50% from the corresponding UV-Vis Spectra of the large particles. For small particles, we observed such shrinkage to be ~9% (Figure 4.4). The shrinkage amount of large particles is consistent with the previous results in polymerized LC films and particles in the nematic phase [64,65] However, the shrinkage behavior of small particles is quite different since the effect of three-dimensional confinement is more pronounced in small particles compared to their larger counterparts, i.e. the surface effects in smaller particles are more critical in defining the shrinkage of small particles. Thus, given the measurements of the shrinkage, we sketch the final shapes of the small and large particles to provide insight into the three-dimensional shapes of the small and large particles as shown in Figure 4.5B and C, respectively.

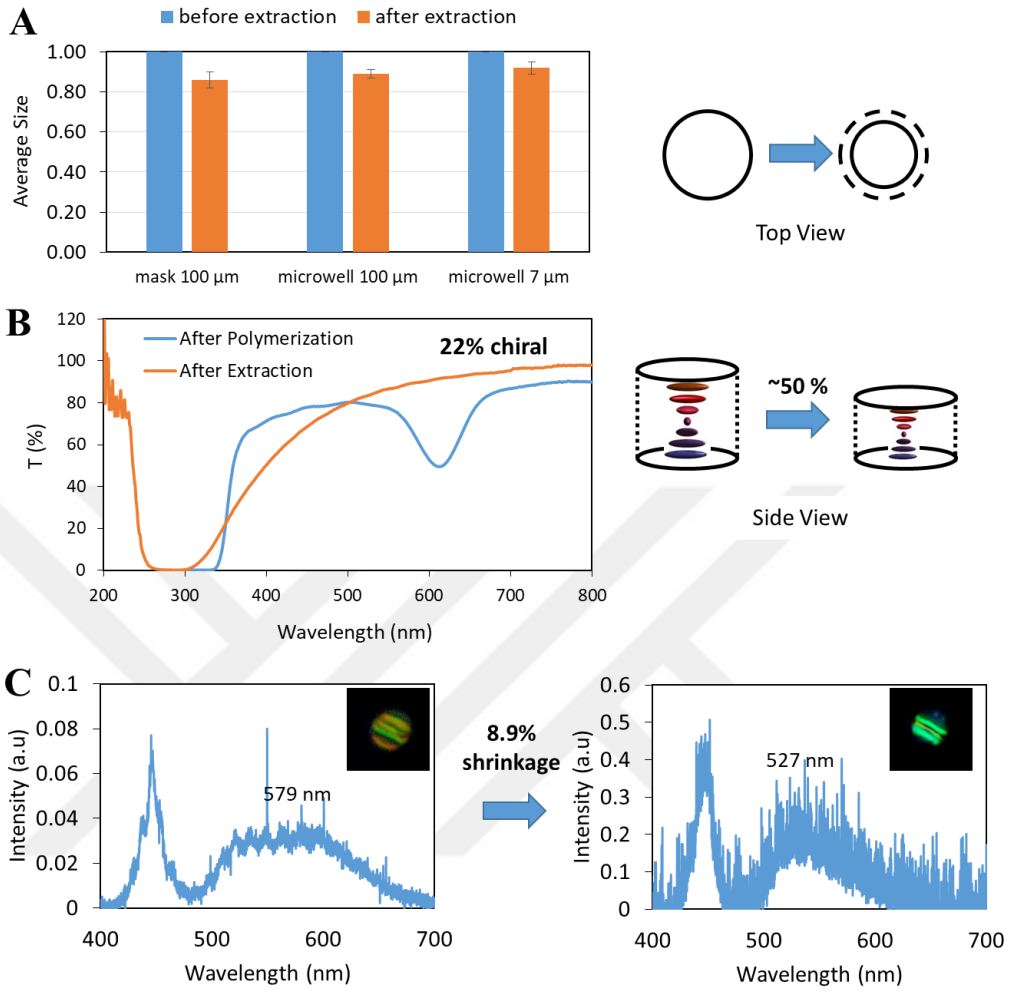

Figure 4.4 Characterizations done for the shrinkage of the particles. (A) Shrinkage amounts of the particles in the radial direction determined from optical micrographs. (B) UV-Vis spectra of the 100 µm sized particles before and after extraction that was used to determine the shrinkage parallel to the cylindrical axis. (C) Reflected light spectra of the 7 µm sized particles before and after extraction that was used to determine the shrinkage parallel to the cylindrical axis.

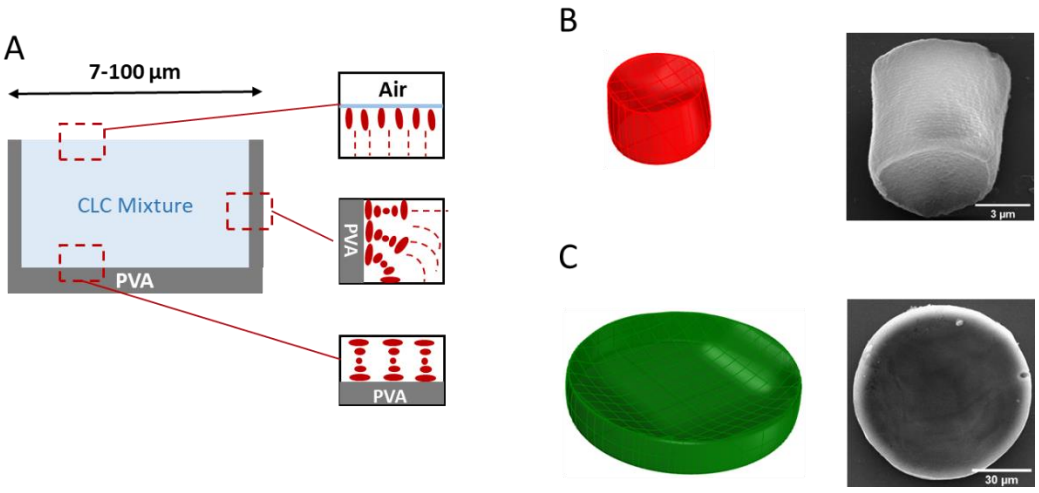

Figure 4.5 (A) A sketch of the LC surface anchoring maintained within the microwells. Sketches of the final shapes (left) and representative SEM micrographs (right) of the small (B) and large particles (C) synthesized by soft lithography method.

We synthesized particles with thicknesses in the range of 1.5–80 µm from the same synthesis mixture (20% wt. RM257 and 8% wt. chiral dopant in E7) to observe whether or not the coloring is influenced by the thickness (or confinement in the vertical direction). Figure 4.6A shows reflection mode polarized optical micrographs of one representative particle for each thickness. We found that the majority of the particles in each set reflected the same color regardless of the thickness they have since the cholesteric template in the structure has the same pitch size.

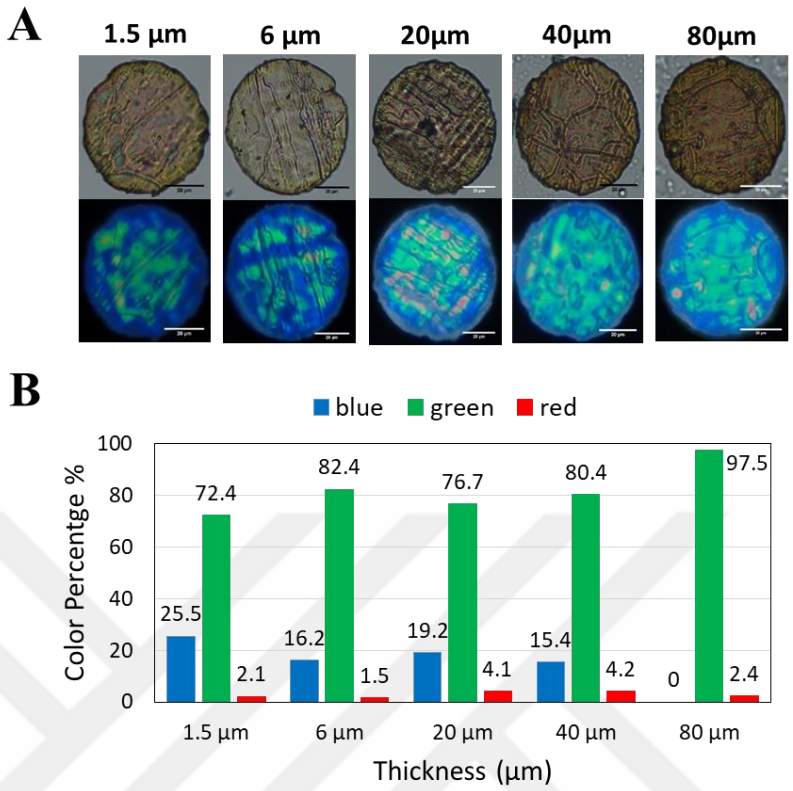

Figure 4.6 (A) Optical microscope images of extracted particles in bright field (top) and in reflection mode (bottom). Particles were synthesized from 20 wt. % RM257 in E7 with 1.5 µm, 6 µm, 20 µm, 40 µm, and 80 µm thicknesses. Thicknesses are i ndicated at the top of the Figure. (B) Color distribution graph as a function of particle thickness.

After completing the characterization studies for round-shaped particles, we synthesized particles in different shapes. We used microwells with two different features as star and triangle shape and polymerized particles from the same synthesis mixture (20% wt. RM257 and 9% wt. chiral dopant in E7). Figure 4.7 shows the microscopy images of extracted particles synthesized by the soft lithography method. Given the shrinkage discussions between the large and small particles that we conducted above, we observed consistency in our results obtained with different shapes. In comparison to the appearances of the star-shaped and triangle-shaped particles synthesized by the soft lithography method, we observed the triangle-shaped particles reflect a higher wavelength than star-shaped particles due to the size

differences. The three-dimensional confinement limited the shrinkage of triangular particles as in small round particles.

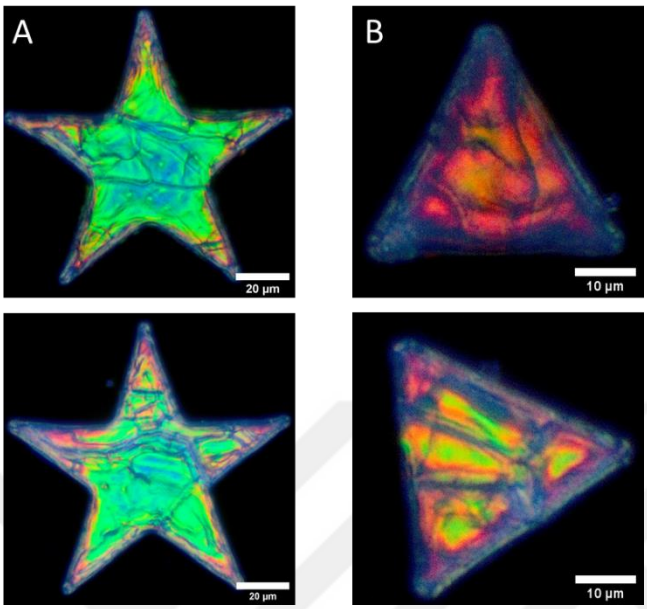

Figure 4.7 Optical microscope images of extracted particles synthesized by soft lithography method. (A) Star shaped (with one side 50µm), and (B) triangle shaped particles (50×50×50 µm).

4.2 Sensor Tests and Response Characteristics of the Particles

We conducted sensor tests using an experimental setup that allows us to control the concentration of toluene. We initially tested particles synthesized from mixtures containing 8% wt. chiral dopant that were characterized as above. During the tests, we collected reflection mode polarized light micrographs at different toluene concentrations in equilibrium with the particles. Figure 4.8 displays representative micrographs of the three types of particles collected during the toluene exposure, showing the color appearance of the particles corresponding to the indicated toluene concentrations. We observed that the coloring of the particles shifted to higher wavelengths with increasing toluene concentration for each case. The red-shift of the reflected color was more significant in large particles even though there was a slight change at low concentration of toluene exposure when scrutinized by the naked eye

(Figure 4.8A and B). However, we barely noticed a color change in small particles even at high concentrations of toluene (Figure 4.8C). After the system was evacuated, we observed a sudden blue-shift of the reflected color which indicates the reversible optical response. However, when the coloring of the particles after the evacuation of the system was compared with their initial optical appearance before toluene exposure, the blue shift of the overall coloring was apparent. This is an indicative of a reduction in the periodicity of the cholesteric twist of the polymer network that may result from a possible shrinkage. We note that we have understood the origin of this observation that we explain below after our careful investigation of the response characteristics and structures of the particles. We note that this is an important observation that helped us understanding the response behavior of the particles.

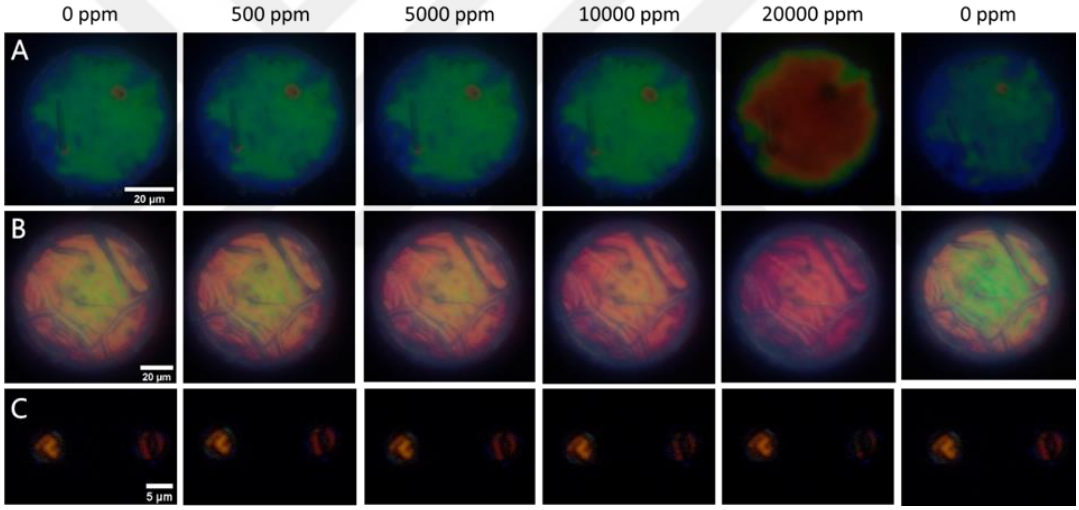

Figure 4.8 Reflection mode optical micrographs of CLC templated polymeric particles collected during sensor tests. (A) particles produced by mask lithography, (B) 100 µm and (C) 7 µm particles produced by soft lithography from a mixture of 20% wt. RM257 and 8% wt. chiral dopant in E7. The values on the top left of each images indicate the concentration of exposed toluene. The leftmost column shows the images of particles before the test and the rightmost column shows the images of particles after removal of toluene. Scale bars: 20 µm for (A) and (B), 5 µm for (C).

To measure the response of the particles against toluene vapor, we quantified the red, green and blue (RGB) signals of collected micrographs using Equation 4 to present our observations. More importantly, using this quantification, we aimed to amplify the color change at low toluene concentrations since we are more interested in the

response at low concentrations. We measured the average RGB values of each particle at different toluene concentrations using imageJ. To highlight both the repeatability and reproducibility of our experiments, we have averaged three independent experiments with three different batches of particles. Each experiment included three independent measurements, each of which included an average of 10 particles. Then, we averaged the sensitivity signal and plotted it with respect to the concentration of toluene to obtain the response curves. Figure 4.9 shows the response curves of the three cases of particles described above. All of the response curves show that the signal gradually increased with the increase in the toluene concentration, consistent with our previous observations on the change of the optical appearance. However, when inspected in more detail and compared the response curves, we arrived to three important features demonstrated within the plots.

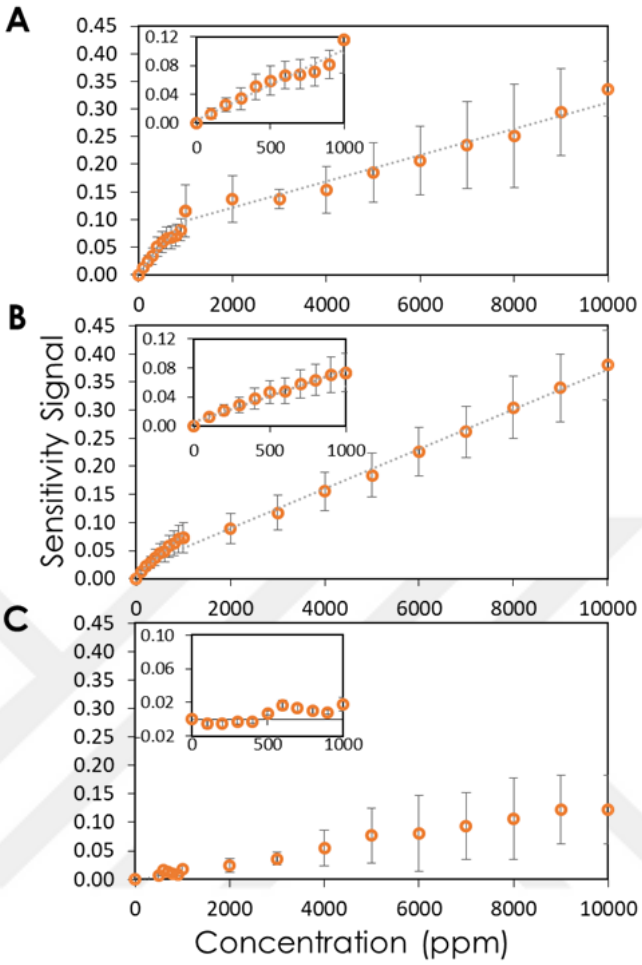

Figure 4.9 Response curves of extracted CLC particles that produced by (A) mask lithography (100 µm) (B) soft lithography (100 µm) (C) soft lithography (7 µm). Insets show the response of the particles up to 1000 ppm of toluene.

First, the response of the large particles prepared with the two different methods were indistinguishable **(**Figure 4.9A, B) showing the minimal effect of the synthesis method of the particles. Second, we observed a more pronounced response of the particles against toluene in the tests with large particles (Figure 4.9A, B) when compared with those of the small particles (Figure 4.9C). Third, the large particles exhibited a response with two trends, however, the small particles exhibit a response with a single trend. Specifically, the slope of the response curve for the large particles

between 0 to 1000 ppm is significantly larger than the slope of the curve between 1000 to 10000 ppm. This two-trend response enhanced the sensitivity of sensor output down to a concentration of 100 ppm (see also the inset in Figure 4.9A, B). Interestingly, when the response curve of 7 μm-size particles was examined, we could not find a significant sensor output in the concentration range of 0-1000 ppm (in Figure 4.9C). When combined, these three major observations are surprising and promising since the sensitivity of the sensor at such low concentrations has not been reported in previous studies conducted by CLCs. At this point, we sought to investigate the underlying phenomena that has led to the abovementioned three observations, which resulted in an increased sensitivity of the sensors leading to the low concentration sensing of VOCs.

We initially reasoned that the low concentration response to originate from the shrinkage that followed the extraction of the unreacted mesogens, since we found the shrinkage extents were significantly different within the small and large particles as reported above. To test this hypothesis, we first performed the toluene exposure experiments with the polymerized particles without the extraction of the unreacted part. In these, we did not observe such a two-trend response as shown in Figure 4.10A. In other words, if the extraction was not performed, the response with high slope at low concentration would not be observed; therefore, high sensitivity would not be achieved at low concentrations. The absence of such a behavior was consistent with our expectation that the extraction step (that led to shrinkage) to play a critical role in the response behavior. Then, to support this result, we produced particles from the mixtures with three different monomer content since the shrinkage was shown to be influenced by the reactive mesogen content in the mixture in polymerized LC films by Karausta et al.[64] We arranged the chiral content according to monomer concentration in the mixture to obtain the same color for each case. When we performed the toluene exposure experiment, we observed the two-trend response for each case but at different slopes, as shown in Figure 4.10B. We were expecting this result since the particles extracted and different monomer concentrations led to different shrinkage percentages.

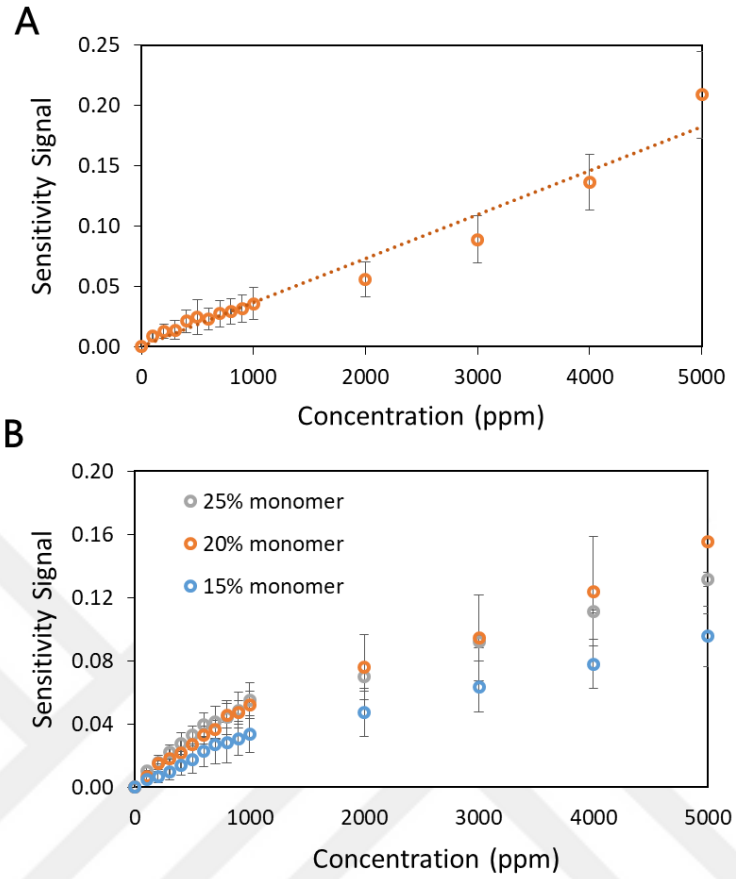

Figure 4.10 Response curves of produced CLC particles by mask lithography (A) not extracted particles, (B) extracted particles produced from mixture of different monomer concentrations.

Then, to establish a more detailed understanding on the characteristics of the particles, we performed thermal characterizations of the polymerized RM257 after extraction of the unreacted mesogens. As shown in the DSC thermogram in Figure 4.11, the polymer exhibited a glass transition (T_g) around 113°C, indicative of the glassy state of the particles at room temperature. Since we performed the extraction of the unreacted mesogens using ethanol as the solvent, which was observed to dissolve the unreacted mesogens but was not absorbed by the polymer[64], we expected the polymer network not to shrink completely. Thus, the polymer may exhibit stored elastic energy due to the glassy state of the polymer, which may result in the abovementioned two trends, low and high concentration, in the response of the large particles.

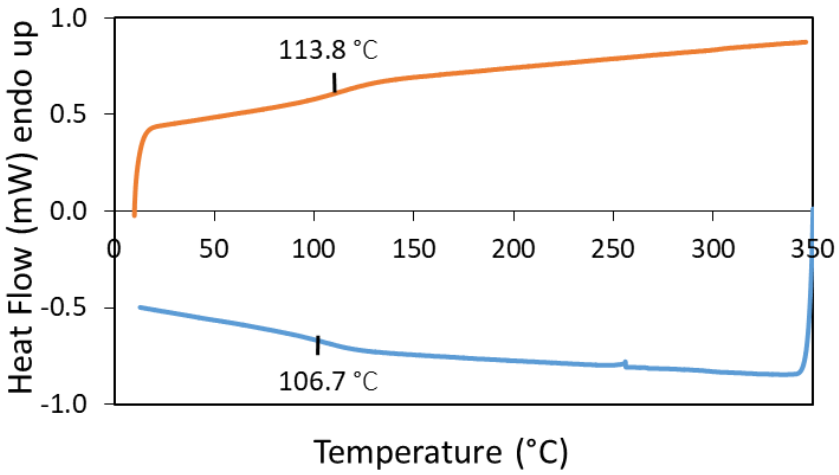

Figure 4.11 Differential Scanning Calorimetry results of polymeric film synthesized from 20% RM257, 8% E7 by weight.

To test the hypothesis of the effect of the stored elastic energy on the response of the particles, we used thermal treatment to anneal the particles and relax the stored elastic energy. The particles were annealed at 150°C (above T_g) overnight before the experiment and then we measured their response at room temperature as shown in Figure 4.12A. Consistent with the other experiments, the thermally annealed particles exhibited a response with single slope showing the diminished effect of the stored elastic energy. As a result of the thermal treatment, polymer chains in rubbery state reorganized, shrunk and released elastic energy. Therefore, we could not see the elastic energy contribution. We also note that the coloring of the particles exhibited a blue shift after thermal annealing (Figure 4.12B) consistent with the further shrinkage of the particles during annealing.

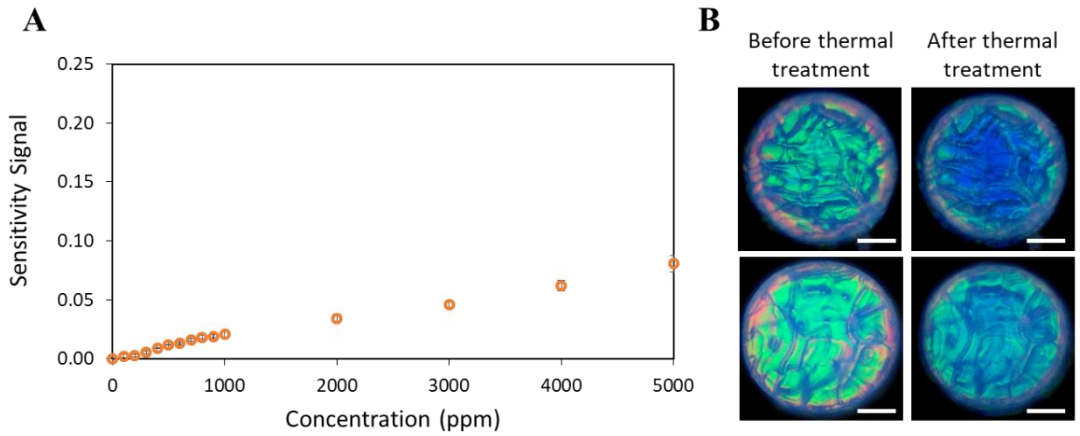

Figure 4.12 (A) Response curves of particles after the thermal annealing test. (B) Reflection mode polarized optical micrographs of two representative particles before and after thermal treatment showing the blue shift of the reflected coloring. The particles were annealed at 150ºC (above T_g) overnight. The images were taken at room temperature. The particles were synthesized from mixtures of 20% RM257, 72% E7, and 8% wt S811. Scale bars: 20 μm.

During the experiments, we observed that the particles did not preserve their original color (slightly blue-shifted, as shown in Figure 4.8A, B) when the system was evacuated after exposure to high concentrations of toluene. For low concentration exposures, however, we observed the particles to restore back to their initial coloring after evacuation of the system from toluene as shown in Figure 4.13A. Then, we performed a set of three-fold control experiments. First, we annealed the particles in high concentrations of toluene to release the elastic energy stored. For this purpose, we exposed the particles in a cycle of three increasing concentrations of toluene. At the end of each test, we evacuated the system and started the exposure from low concentrations of toluene. We first measured the response of the particles against toluene concentrations up to 5000 ppm. Then, we performed the second measurement up to a toluene concentration of 20000 ppm (saturation concentration). Lastly, we repeated the measurement up to 5000 ppm after evacuation to compare with the first run. When we compared the sensitivity signals as shown in Figure 4.13B, we found that the two-trend response was apparent in the first two runs, however, it was absent in the third run replacing with a sensitivity curve with a single

slope. This result, consistently with the observation in Figure 4.13A, is an indicative of the release of the elastic energy stored within the polymer network after plasticization with high concentrations of toluene.

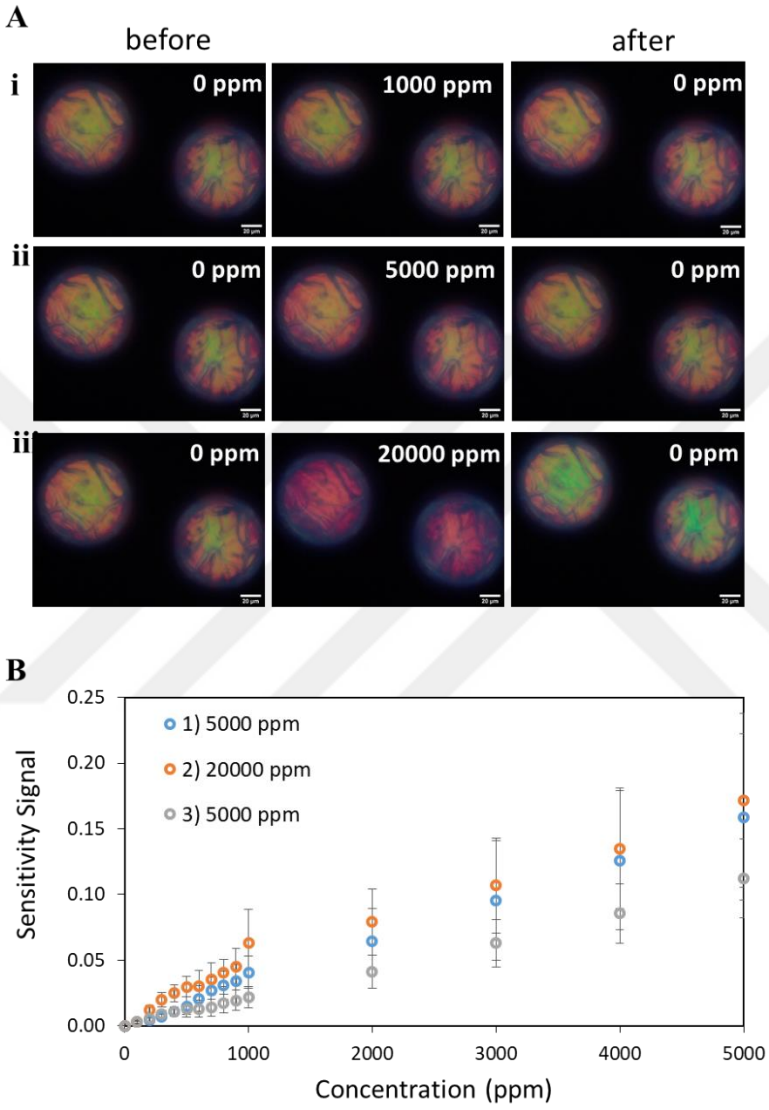

Figure 4.13 (A) Reflection mode polarized optical micrographs of the particles before, during and after the exposure to toluene. The particles were exposed to (i) 1000 ppm, (ii) 5000 ppm toluene, and (iii) 20000 ppm. The images in the right column were taken after the system was evacuated from toluene. (A) Chemical annealing test. The particles were synthesized from mixtures of 20% RM257, 72% E7, and 8% wt S811. Scale bars: 20 µm.

With the comprehensive control experiments explained above, we showed that the particles templated from CLCs exhibit a more sensitive response to the VOCs due to the stored elastic energy. We highlight here that the elastic energy was stored in the polymer matrix during the extraction of the unreacted mesogens using ethanol that is not absorbed by the polymer matrix. When we performed the extraction of the unreacted mesogens using toluene which is also known to plasticize the polymerized RM257, we observed that the sensitive response of the polymer was lost due to the disappearance of the stored elastic energy within the polymer network (Figure 4.14). Thus, we found herein that the extraction of the unreacted mesogens is an important and a critical step in our synthesis procedure that led to the above explained two-trend response against toluene.

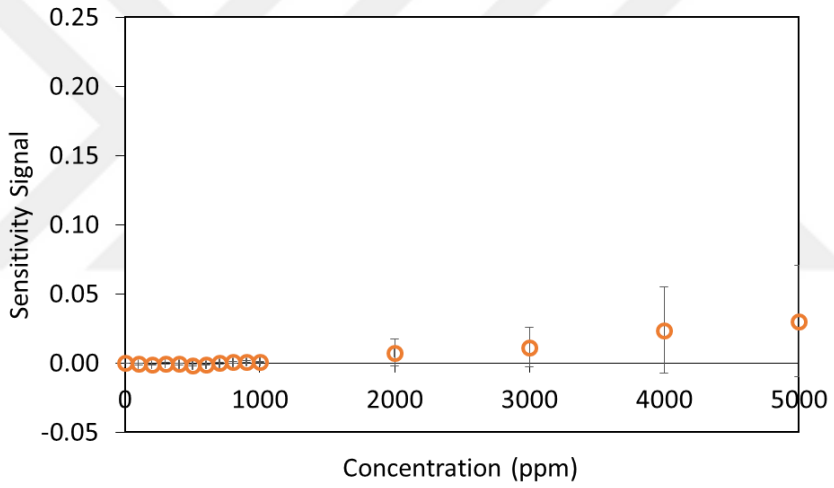

Figure 4.14 Toluene response curves of the 100 µm-sized CLC particles synthesized by mask lithography method and extracted using toluene. The particles were synthesized from mixtures of 20% wt RM257, 74% wt E7, 6% wt S811.

We comment on the low sensitivity of the smaller sized particles that were apparent in the toluene exposure experiments shown in Figure 4.8C. The lower sensitivity signal in toluene exposure experiments with smaller sized particles synthesized with soft lithography results from the lower shrinkage of the particles after extraction step. As we have mentioned in the characterization part, such particles exhibited limited shrinkage after the extraction step due to the polymer chain alignment maintained

within the particles. Such behavior, as expected, then did not result in the storage of an elastic energy within the particles and thus led to a response with a single slope.

Lastly, we tested star and triangle-shaped particles upon toluene exposure. We obtained a perfect two-trend response when we tested the star-shaped particles while we could not observe any significant response with triangle-shaped ones, in the concentration range of 0-1000 ppm (Figure 4.15). We proved once again that if the shrinkage of particle is limited by the confinement, the elastic energy contribution disappears from the sensor output.

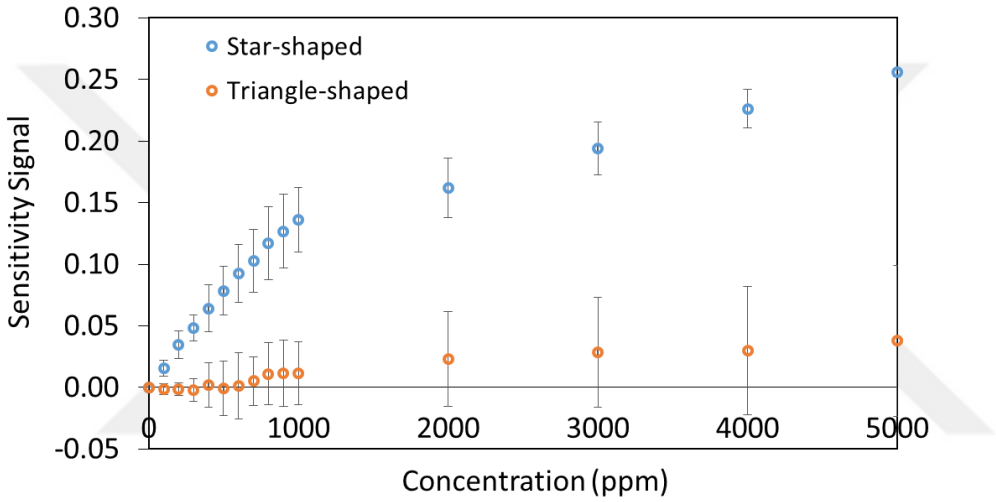

Figure 4.15 Response curves of different shape (star and triangle) CLC particles synthesized by soft lithography.

4.3 Integration of Sensors in a Chip Form

After the observation of the enhanced response of the particles templated from CLCs to a high sensitivity that covers the concentrations set by regulations, herein we aimed to design our sensors in a form that would be more reliable, more quantifiable and in a geometry that would enable integration into devices for our ultimate goal of developing easy-to-use, wearable optical sensors. We were motivated to design such a system that offers an easy collection of data from a large number of particles at the same time, therefore enabling the users to obtain statistical data for more reliable measurements. Thus, we modified our methods to synthesize particles that are

covalently bonded to the glass substrate underneath to immobilize particles that were far apart from each other to track the changes in each of them precisely. Although the advantageous elastic energy that was affecting the response characteristics of the particles were due to the shrinkage in a direction along the cholesteric axis, we were initially cautious on whether or not the appearance of the particles would be affected by such immobilization and whether or not their response will be preserved after immobilization onto glass substrates. For the immobilization of the particles on glass surfaces, we initially functionalized one of the glass surfaces with 3-(trichlorosilyl)propyl methacrylate (TCSPM) to provide a surface with acrylate groups that can crosslink with RM257 during the synthesis of the particles using mask lithography. We synthesized the immobilized particles using a mixture of 20% wt. RM257 and 6% wt. chiral dopant in E7. After extraction, the coloring of the particles was evident in the optical micrographs shown in Figure 4.16A. We conducted sensor tests again as three independent experiments with three different batches of approximately 30 particles. During exposure to toluene vapor, the immobilized particles exhibited a red-shift of the reflected color as shown in Figure 4.16A, similar to those we observed for the free particles we explained above. The two-trend response was present upon toluene exposure (Figure 4.16B and 4.16C). Thus, the sensitivity was enough to reliably determine the concentration of toluene in the range of 0-1000 ppm. When we inspected the response curves of the immobilized particles in comparison with those of the free particles shown above (Figure 4.9A and 4.9B), we obtained more accurate results in the case of the immobilized particles. To compare the statistics of the response of the immobilized and free particles, we calculated the coefficient of variance (CV), which indicates a measure of the dispersion of the average signal values. Such calculations revealed that CV of response of immobilized particles was 18.1% while that of the free particles synthesized with mask lithography and soft lithography methods were

32.6% and 32.5%, respectively, showing a significant improvement in the accuracy of the measurements with the immobilized particles.

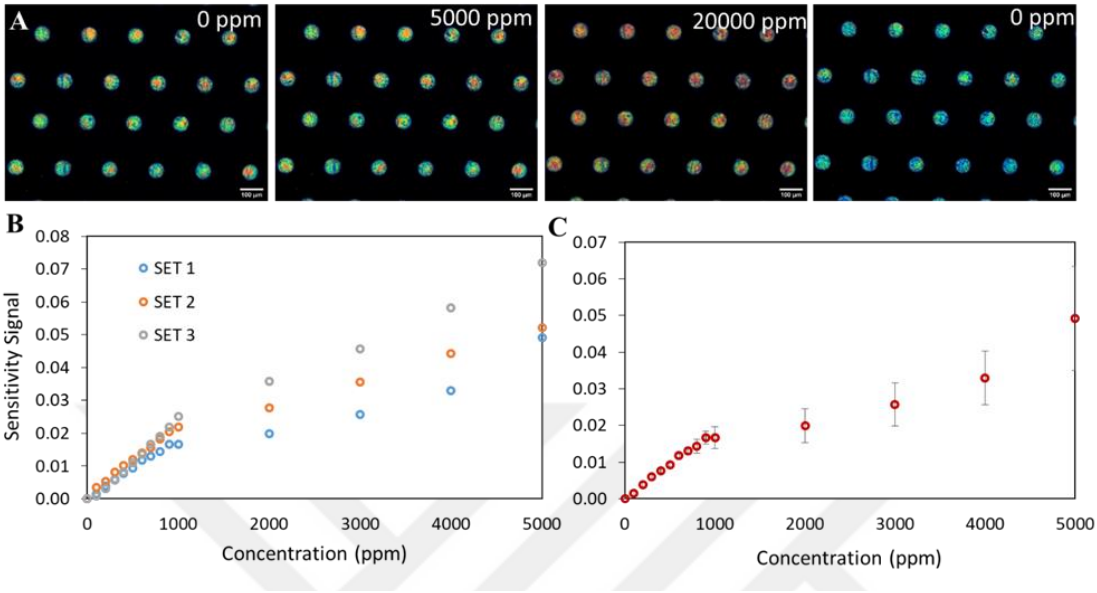

Figure 4.16 Reflection mode polarized optical micrographs of CLC templated polymeric particles produced by mask lithography covalently bonded to the surface with acrylate monolayer (A) before, during and after toluene exposure. Response curves of the CLC particles against toluene vapor demonstrating (B) each set with three different batches of approximately 30 particles and (C) average of three-set. Scale bars: 100 μm.

After obtaining a significantly better sensitivity using the immobilized particles, we performed a time-dependent sensor tests with the immobilized particles to simulate a real-time use of our sensor chips. We designed cyclic experiments with alternating exposure of toluene and evacuating the system in between, aiming to test response time and sensor reusability. We exposed the particles to toluene vapor as a step input of 500 ppm with a profile as shown with straight lines in Figure 4.17 and measured the response of particles with time. We measured the response signal and converted it to concentration and plotted our measured concentrations as shown in Figure 4.17 (data points).

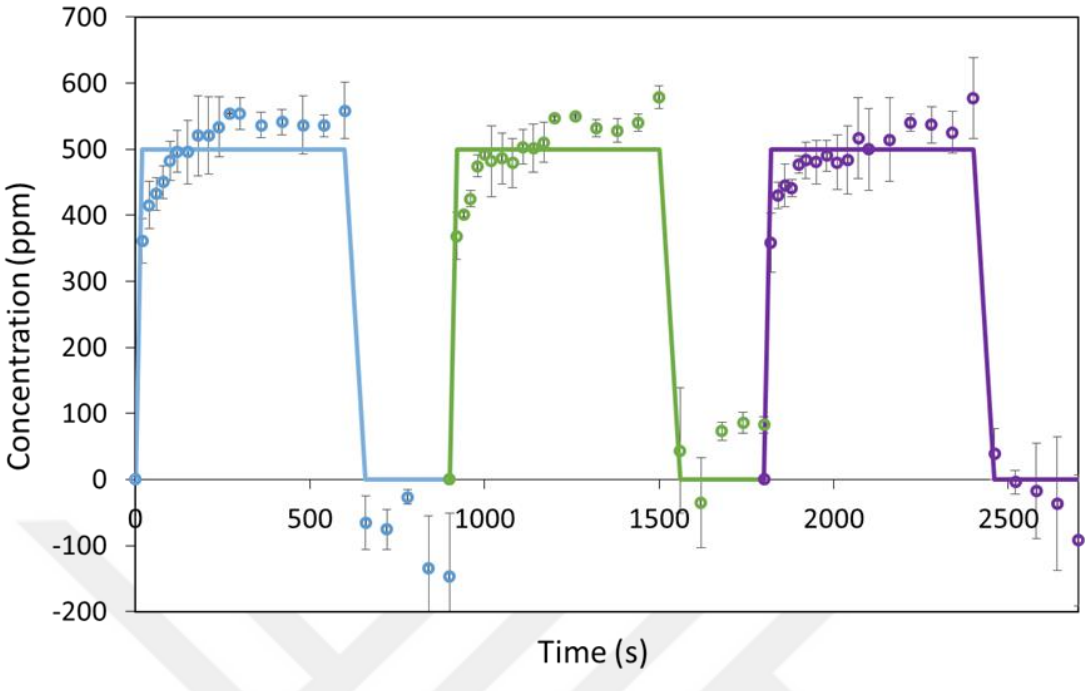

Figure 4.17 Alternating exposed (toluene exposure for 10 min) and evacuated (removing toluene for 5 min) measurements of the sensor output (data points) together with exposure profile (straight lines).

We found that the particles responded instantaneously to toluene as soon as it was introduced into the system. Within 20 seconds, we measured ~70% of the equilibrium response to be reached, and the equilibrium response was reached in less than 2 minutes as shown in Figure 4.17. Moreover, we determined the total exposed amount as 3×10^5 ppm·s within 10 minutes of exposure, that is 100.1 ± 1.2% of the amount calculated relative to the theoretical amount of toluene introduced to the system. As shown in the Figure 4.17, we also did not observe any loss or change in the equilibrium response of the particles within each cycle showing the reusability of the sensors.

Herein, we want to mention another experiment that we conducted for the reusability of the sensors. For this, we chose a set of particles synthesized within microwells and tried upon toluene exposure ten times in a row and did not observe any distortion or decrease in the response even when we used the same sample ten months later as shown in Figure 4.18.

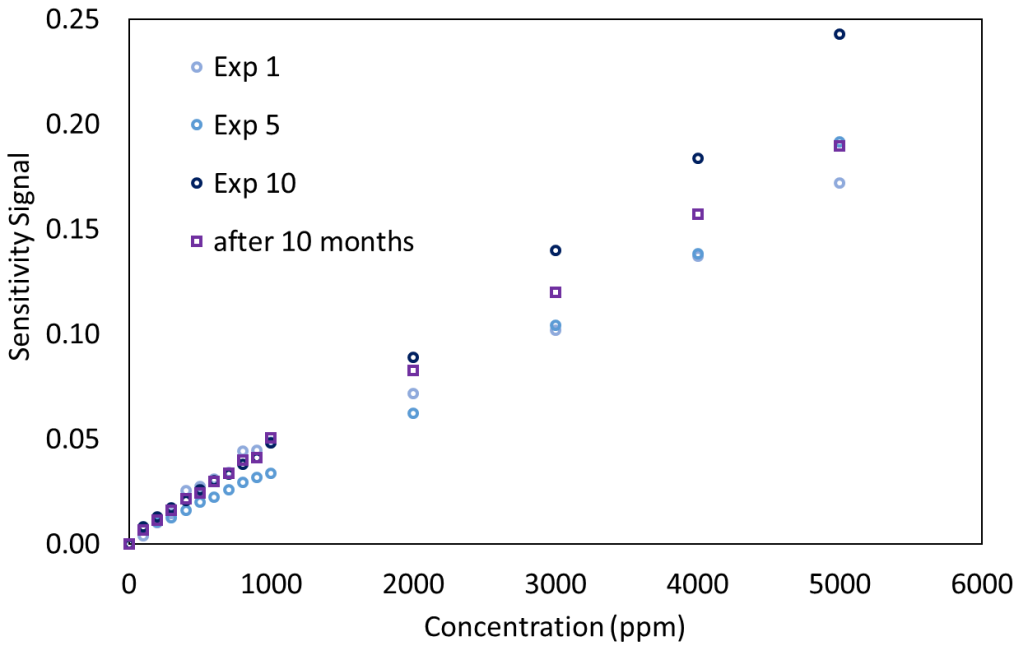

Figure 4.18 Response curves of CLC templated particles produced by soft lithography from reusability tests (circles belongs to ten times trial, square belongs to test after 10 months).

Overall, these experiments we conducted herein, proved the reversibility, reusability and reliability of our sensors in determination of the toluene concentrations in the level of 100 ppm, which is critical for health and safety concerns.

CHAPTER 5

CONCLUSION

The particles synthesized using cholesteric LCs were able to detect volatile organic compounds at the concentration in the order of 100 ppm, which also enable rapid, reusable, and sensitive detection through easy monitoring simply by a photo camera. We have demonstrated that the details in the synthesis of the particles from cholesteric LCs to play a critical role in the sensitivity of the particles. Specifically, we have observed a direct relation between the elastic energy stored in the cholesteric structure and the sensitivity of the sensor. We found that the elastic energy was associated to the shrinkage of the particles resulting from the deswelling of the particles after extraction of the unreacted mesogens. The chemical used in the extraction step appeared to be critical in the sensitivity as it requires a solvent that does not exhibit significant partitioning in the polymer matrix. Otherwise, partitioning of solvent in the polymer during extraction may lead to plasticization of the polymer resulting in disappearance of the elastic energy stored in the polymer matrix. Overall, the results reported herein supports that the elastic energy resulting from the anisotropy in the polymer matrix to significantly enhance the sensitivity of the sensors that may not be possible with the isotropic molecular templates. This study demonstrated the sensitivity of the polymeric sensors synthesized from cholesteric LC templates, with no control over the magnitude of the elastic energy stored in the polymer matrix, thus, future studies may benefit from such investigations to further enhance the sensitivity of the sensors. In addition, the diversity of the LC ordering may also be employed to improve their sensor properties.

REFERENCES

(1) Dumanli, A. G.; Savin, T. Recent Advances in the Biomimicry of Structural Colours. *Chemical Society Reviews*. 2016,24, 6698-6724.

(2) Zhao, Y.; Xie, Z.; Gu, H.; Zhu, C.; Gu, Z. Bio-Inspired Variable Structural Color Materials. *Chemical Society Reviews*. 2012, 41, 3297-3317.

(3) Kinoshita, S.; Yoshioka, S.; Miyazaki, J. Physics of Structural Colors. *Reports Prog. Phys.* 2008, 71, 076401.

(4) Sun, J.; Bhushan, B.; Tong, J. Structural Coloration in Nature. *RSC Advances*. 2013, 3, 14862.

(5) Vigneron, J. P.; Simonis, P. Structural Colours. In *Advances in Insect Physiology*; 2010, 38, 81-218.

(6) Shawkey, M. D.; D'Alba, L. Interactions between Colour-Producing Mechanisms and Their Effects on the Integumentary Colour Palette. *Philosophical Transactions of the Royal Society B: Biological Sciences*. 2017, 372, 20160536.

(7) Yu, K.; Fan, T.; Lou, S.; Zhang, D. Biomimetic Optical Materials: Integration of Nature's Design for Manipulation of Light. *Progress in Materials Science*. 2013,58,825-873.

(8) Zyla, G.; Kovalev, A.; Grafen, M.; Gurevich, E. L.; Esen, C.; Ostendorf, A.; Gorb, S. Generation of Bioinspired Structural Colors via Two-Photon Polymerization. *Sci. Rep.* 2017,7,1-9.

(9) Butt, H.; Yetisen, A. K.; Mistry, D.; Khan, S. A.; Hassan, M. U.; Yun, S. H. Morpho Butterfly-Inspired Nanostructures. *Adv. Opt. Mater.* 2016, 4, 497-504.

(10) Fenzl, C.; Hirsch, T.; Wolfbeis, O. S. Photonic Crystals for Chemical Sensing and Biosensing. *Angewandte Chemie - International Edition*. 2014, 53, 3318-3335.

(11) Cong, H.; Yu, B.; Zhao, X. S. Imitation of Variable Structural Color in Paracheirodon Innesi Using Colloidal Crystal Films. *Opt. Express*. 2011, 19, 12799-12808.

(12) Yoshioka, S.; Matsuhana, B.; Tanaka, S.; Inouye, Y.; Oshima, N.; Kinoshita, S. Mechanism of Variable Structural Colour in the Neon Tetra: Quantitative Evaluation of the Venetian Blind Model. *J. R. Soc. Interface.* 2011,8,56-66.

(13) Teyssier, J.; Saenko, S. V.; Van Der Marel, D.; Milinkovitch, M. C. Photonic Crystals Cause Active Colour Change in Chameleons. *Nat. Commun.* 2015, 6, 1-7.

(14) Bukusoglu, E.; Bedolla Pantoja, M.; Mushenheim, P. C.; Wang, X.; Abbott, N. L. Design of Responsive and Active (Soft) Materials Using Liquid Crystals. *Annu. Rev. Chem. Biomol. Eng.* 2016,7,163-196.

(15) Wang, L.; Urbas, A. M.; Li, Q. Nature-Inspired Emerging Chiral Liquid Crystal Nanostructures: From Molecular Self-Assembly to DNA Mesophase and Nanocolloids. *Adv. Mater.* 2018,1801335.

(16) White, T. J.; McConney, M. E.; Bunning, T. J. Dynamic Color in Stimuli-Responsive Cholesteric Liquid Crystals. *J. Mater. Chem.* 2010,20,9832-9847.

(17) Mulder, D. J.; Schenning, A. P. H. J.; Bastiaansen, C. W. M. Chiral-Nematic Liquid Crystals as One Dimensional Photonic Materials in Optical Sensors. *J. Mater. Chem. C.* 2014, 2, 6695-6705.

(18) Herzer, N.; Guneysu, H.; Davies, D. J. D.; Yildirim, D.; Vaccaro, A. R.; Broer, D. J.; Bastiaansen, C. W. M.; Schenning, A. P. H. J. Printable Optical Sensors Based on H-Bonded Supramolecular Cholesteric Liquid Crystal Networks. *J. Am. Chem. Soc.* 2012, 134, 7608-7611.

(19) Picot, O. T.; Dai, M.; Billoti, E.; Broer, D. J.; Peijs, T.; Bastiaansen, C. W. M. A Real Time Optical Strain Sensor Based on a Cholesteric Liquid Crystal Network. *RSC Adv.* 2013, 3, 18794-18798.

(20) Mujahid, A.; Stathopulos, H.; Lieberzeit, P. A.; Dickert, F. L. Solvent Vapour

Detection with Cholesteric Liquid Crystals-Optical and Mass-Sensitive Evaluation of the Sensor Mechanism. *Sensors* 2010, 10, 4887-4897.

(21) Moirangthem, M.; Scheers, A. F.; Schenning, A. P. H. J. A Full Color Photonic Polymer, Rewritable with a Liquid Crystal Ink. *Chem. Commun.* 2018, 54, 4425-4428.

(22) Sutarlie, L.; Qin, H.; Yang, K. L. Polymer Stabilized Cholesteric Liquid Crystal Arrays for Detecting Vaporous Amines. *Analyst.* 2010, 135, 1691-1696.

(23) Chang, C. K.; Bastiaansen, C. W. M.; Broer, D. J.; Kuo, H. L. Discrimination of Alcohol Molecules Using Hydrogen-Bridged Cholesteric Polymer Networks. *Macromolecules.* 2012, 45, 4550-4555.

(24) Esteves, C.; Ramou, E.; Porteira, A. R. P.; Moura Barbosa, A. J.; Roque, A. C. A. Seeing the Unseen: The Role of Liquid Crystals in Gas-Sensing Technologies. *Advanced Optical Materials*. 2020, 8, 1902117.

(25) Lockwood, N. A.; Gupta, J. K.; Abbott, N. L. Self-Assembly of Amphiphiles, Polymers and Proteins at Interfaces between Thermotropic Liquid Crystals and Aqueous Phases. *Surface Science Reports*. 2008.

(26) OSHA. Safety and Health Topics | Toluene - Occupational Exposure Limits | Occupational Safety and Health Administration.

(27) Mirzaei, A.; Kim, J. H.; Kim, H. W.; Kim, S. S. Resistive-Based Gas Sensors for Detection of Benzene, Toluene and Xylene (BTX) Gases: A Review. *Journal of Materials Chemistry C*. 2018, 6, 4342-4370.

(28) Allouch, A.; Le Calvé, S.; Serra, C. A. Portable, Miniature, Fast and High Sensitive Real-Time Analyzers: BTEX Detection. *Sensors and Actuators, B: Chemical*. 2013, 182, 446-452.

(29) Khan, S.; Newport, D.; Le Calvé, S. Development of a Toluene Detector Based on Deep UV Absorption Spectrophotometry Using Glass and Aluminum Capillary Tube Gas Cells with a LED Source. *Micromachines.*

2019, 10, 193.

(30) Jalal, A. H.; Alam, F.; Roychoudhury, S.; Umasankar, Y.; Pala, N.; Bhansali, S. Prospects and Challenges of Volatile Organic Compound Sensors in Human Healthcare. *ACS Sensors*. 2018, 3, 1246-1263.

(31) Szulczyński, B.; Gębicki, J. Currently Commercially Available Chemical Sensors Employed for Detection of Volatile Organic Compounds in Outdoor and Indoor Air. *Environments.* 2017, 4, 21.

(32) Zampolli, S.; Elmi, I.; Mancarella, F.; Betti, P.; Dalcanale, E.; Cardinali, G. C.; Severi, M. Real-Time Monitoring of Sub-Ppb Concentrations of Aromatic Volatiles with a MEMS-Enabled Miniaturized Gas-Chromatograph. *Sensors Actuators, B Chem.* 2009, 141, 322-328.

(33) Huang, G.; Gao, L.; Duncan, J.; Harper, J. D.; Sanders, N. L.; Ouyang, Z.; Cooks, R. G. Direct Detection of Benzene, Toluene, and Ethylbenzene at Trace Levels in Ambient Air by Atmospheric Pressure Chemical Ionization Using a Handheld Mass Spectrometer. *J. Am. Soc. Mass Spectrom.* 2011, 21, 132-135.

(34) Lara-Lbeas, I.; Rodríguez-Cuevas, A.; Andrikopoulou, C.; Person, V.; Baldas, L.; Colin, S.; Calvé, S. Le. Sub-Ppb Level Detection of BTEX Gaseous Mixtures with a Compact Prototype GC Equipped with a Preconcentration Unit. *Micromachines.* 2019, 10, 187.

(35) Spinelle, L.; Gerboles, M.; Kok, G.; Persijn, S.; Sauerwald, T. Review of Portable and Low-Cost Sensors for the Ambient Air Monitoring of Benzene and Other Volatile Organic Compounds. *Sensors*. 2017, 17, 1520.

(36) Sekhar, P. K.; Subramaniyam, K. Detection of Harmful Benzene, Toluene, Ethylbenzene, Xylenes (BTEX) Vapors Using Electrochemical Gas Sensors. *ECS Electrochem. Lett.* 2014, 3, B1-B4.

(37) Ho, C. K.; Itamura, M. T.; Kelley, M.; Hughes, R. C. Review of Chemical Sensors for In-Situ Monitoring of Volatile Contaminants. *Contract.* 2001, 28.

(38) Coelho Rezende, G.; Le Calvé, S.; Brandner, J. J.; Newport, D. Micro Photoionization Detectors. *Sensors and Actuators, B: Chemical*. 2019, 287, 86-94.

(39) Li, Y.; Chen, N.; Deng, D.; Xing, X.; Xiao, X.; Wang, Y. Formaldehyde Detection: SnO2 Microspheres for Formaldehyde Gas Sensor with High Sensitivity, Fast Response/Recovery and Good Selectivity. *Sensors Actuators, B Chem.* 2017, 238, 264-273.

(40) Lin, T.; Lv, X.; Hu, Z.; Xu, A.; Feng, C. Semiconductor Metal Oxides as Chemoresistive Sensors for Detecting Volatile Organic Compounds. *Sensors*. 2019, 19, 233.

(41) Tang, W.; Wang, J. Mechanism for Toluene Detection of Flower-like ZnO Sensors Prepared by Hydrothermal Approach: Charge Transfer. *Sensors Actuators, B Chem.* 2015, 207, 66-73.

(42) Xiao, Y.; Yu, J.; Shun, L.; Tan, S.; Cai, X.; Luo, Y.; Zhang, J.; Dong, H.; Lu, H.; Guan, H.; Zhong, Y.; Tang, J.; Chen, Z. Reduced Graphene Oxide for Fiber-Optic Toluene Gas Sensing. *Opt. Express.* 2016, 24, 28290-28302.

(43) Kek, K. J.; Lee, J. J. Z.; Otono, Y.; Ishihara, S. Chemical Gas Sensors Using Chiral Nematic Liquid Crystals and Its Applications. *J. Soc. Inf. Disp.* 2017, 25, 366-373.

(44) Matejec, V.; Mrazek, J.; Podrazky, O.; Hayer, M.; Pospisilova, M. Fiber-Optic U-Shaped Detection Elements for the Investigation of Photocatalytic Activity of Optical Fibers Coated with Layer of TiO2. *Sens. Lett.* 2009, 7, 900-904.

(45) Hromadka, J.; Korposh, S.; Partridge, M.; James, S. W.; Davis, F.; Crump, D.; Tatam, R. P. Volatile Organic Compounds Sensing Using Optical Fibre Long Period Grating with Mesoporous Nano-Scale Coating. *Sensors*. 2017, *17*, 205.

(46) Tang, J.; Fang, J.; Liang, Y.; Zhang, B.; Luo, Y.; Liu, X.; Li, Z.; Cai, X.; Xian,

J.; Lin, H.; Zhu, W.; Guan, H.; Lu, H.; Zhang, J.; Yu, J.; Chen, Z. All-Fiber-Optic VOC Gas Sensor Based on Side-Polished Fiber Wavelength Selectively Coupled with Cholesteric Liquid Crystal Film. *Sensors Actuators, B Chem.* 2018, 273, 1816-1826.

(47) Athanasekos, L.; Pispas, S.; Riziotis, C. Novel Block Copolymers for Multi-Agent Detection Using Polymer Optical Fibers. *Microstruct. Spec. Opt. Fibres* 2012, 8426, 842615.

(48) Kou, D.; Ma, W.; Zhang, S.; Tang, B. Copolymer-Based Photonic Crystal Sensor for Discriminative Detection of Liquid Benzene, Toluene, Ethylbenzene, and Xylene. *ACS Appl. Polym. Mater*. 2020, 2, 2-11.

(49) Chang, H.; Chang, G. T.; Thokchom, A. K.; Kim, T.; Park, J. Ultra-Fast Responsive Colloidal – Polymer Composite-Based Volatile Organic Compounds (VOC) Sensor Using Nanoscale Easy Tear Process. *Sci. Rep.* 2018, 8 , 1–11

(50) Dolai, S.; Bhurnia, S. K.; Beglaryan, S. S.; Kolusheva, S.; Zeiri, L.; Jelinek, R. Colorimetric Polydiacetylene − Aerogel Detector for Volatile Organic Compounds (VOCs). *Appl. Mater. Interfaces* 2017, *9*, 2891–2898.

(51) Wang, Y.; Zhong, X.; Huo, D.; Zhao, Y.; Geng, X.; Fa, H.; Luo, X.; Yang, M.; Hou, C. Fast Recognition of Trace Volatile Compounds with a Nanoporous Dyes-Based Colorimetric Sensor Array. *Talanta.* 2019, 192, 407-417.

(52) Azzouz, A.; Kumar, V.; Kim, K. H.; Ballesteros, E.; Rhadfi, T.; Malik, A. K. Advances in Colorimetric and Optical Sensing for Gaseous Volatile Organic Compounds. *TrAC - Trends in Analytical Chemistry*. 2019, 118, 205-516.

(53) Askim, J. R.; Mahmoudi, M.; Suslick, K. S. Optical Sensor Arrays for Chemical Sensing: The Optoelectronic Nose. *Chemical Society Reviews*. 2013, 42, 8649-8682.

(54) Nayani, K.; Rai, P.; Bao, N.; Yu, H.; Mavrikakis, M.; Twieg, R. J.; Abbott,

N. L. Liquid Crystals with Interfacial Ordering That Enhances Responsiveness to Chemical Targets. *Adv. Mater.* 2018, *30*, 1–7.

(55) Bedolla Pantoja, M. A.; Abbott, N. L. Surface-Controlled Orientational Transitions in Elastically Strained Films of Liquid Crystal That Are Triggered by Vapors of Toluene. *ACS Appl. Mater. Interfaces.* 2016, 8, 13114-13122.

(56) Hunter, J. T.; Abbott, N. L. Adsorbate-Induced Anchoring Transitions of Liquid Crystals on Surfaces Presenting Metal Salts with Mixed Anions. *ACS Appl. Mater. Interfaces.* 2014, 6, 2362-2369.

(57) Reyes, C. G.; Sharma, A.; Lagerwall, J. P. F. Non-Electronic Gas Sensors from Electrospun Mats of Liquid Crystal Core Fibres for Detecting Volatile Organic Compounds at Room Temperature. *Liq. Cryst.* 2016, 43,1986-2001.

(58) Wang, J.; Jákli, A.; West, J. L. Liquid Crystal/Polymer Fiber Mats as Sensitive Chemical Sensors. *J. Mol. Liq.* 2018, 267, 490-495.

(59) Guan, Y.; Agra-Kooijman, D. M.; Fu, S.; Jákli, A.; West, J. L. Responsive Liquid-Crystal-Clad Fibers for Advanced Textiles and Wearable Sensors. *Adv. Mater.* 2019, 31, 1902168.

(60) Han, Y.; Pacheco, K.; Bastiaansen, C. W. M.; Broer, D. J.; Sijbesma, R. P. Optical Monitoring of Gases with Cholesteric Liquid Crystals. *J. Am. Chem. Soc.* 2010, 132, 2961-2967.

(61) Sutarlie, L.; Lim, J. Y.; Yang, K. L. Cholesteric Liquid Crystals Doped with Dodecylamine for Detecting Aldehyde Vapors. *Anal. Chem.* 2011, 83, 5253-5258.

(62) Winterbottom, D. A.; Narayanaswamy, R.; Jr, I. M. R. Cholesteric Liquid Crystals for Detection of Organic Vapours. *Sens. Actuators, B.* 2003, *90*, 52–57.

(63) Chang, C. K.; Kuo, H. L.; Tang, K. T.; Chiu, S. W. Optical Detection of Organic Vapors Using Cholesteric Liquid Crystals. *Appl. Phys. Lett.* 2011, *99*, 10–13.

(64) Karausta, A.; Bukusoglu, E. Liquid Crystal-Templated Synthesis of Mesoporous Membranes with Predetermined Pore Alignment. *ACS Appl. Mater. Interfaces* 2018, 10, 33484-33492.

(65) Akdeniz, B.; Bukusoglu, E. Liquid Crystal Templates Combined with Photolithography Enable Synthesis of Chiral Twisted Polymeric Microparticles. *Macromol. Rapid Commun.* 2019, 40, 1900160.

(66) Wang, X.; Bukusoglu, E.; Abbott, N. L. A Practical Guide to the Preparation of Liquid Crystal-Templated Microparticles. *Chemistry of Materials*. 2017,29,53-61.

(67) Akdeniz, B.; Bukusoglu, E. Design Parameters and Principles of Liquid-Crystal-Templated Synthesis of Polymeric Materials via Photolithography. *Langmuir* 2019,35,13126-13134.